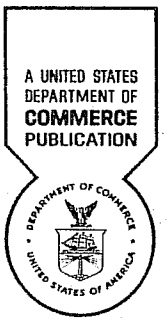

ESSA RESEARCH LABORATORIES
Air Resources Laboratories
Silver Spring, Maryland
January 1970

Atmospheric Transport and Diffusion in the Planetary Boundary Layer

Technical Memorandum ERLTM-ARL 17

U.S. DEPARTMENT OF COMMERCE / ENVIRONMENTAL SCIENCE SERVICES ADMINISTRATION

ESSA RESEARCH LABORATORIES

AIR RESOURCES LABORATORIES

IMPORTANT NOTICE

Technical Memoranda are used to insure prompt dissemination of special studies which, though of interest to the scientific community, may not be ready for formal publication. Since these papers may later be published in a modified form to include more recent information or research results, abstracting, citing, or reproducing this paper in the open literature is not encouraged. Contact the author for additional information on the subject matter discussed in this Memorandum.

U.S. DEPARTMENT OF COMMERCE
Environmental Science Services Administration
Research Laboratories

ESSA Technical Memorandum ERLTM-ARL 17

ATMOSPHERIC TRANSPORT AND DIFFUSION IN THE PLANETARY BOUNDARY LAYER

I. Van der Hoven, Editor

Contributors

J. K. Angell
A. B. Bernstein
D. J. Bjorem
C. R. Dickson
E. H. Markee
D. H. Pack
G. E. Start
L. L. Wendell

Semiannual Research Program Review
January - June 1969
U. S. Atomic Energy Commission

Air Resources Laboratory
Silver Spring, Maryland
January 1970

PREFACE

In accordance with the letter of agreement of July 15, 1968, with the U. S. Atomic Energy Commission, Division of Reactor Development and Technology, Environmental and Sanitary Engineering Branch, the Air Resources Laboratories have continued their study of atmospheric transport and diffusion in the planetary boundary layer, micrometeorology, diffusion climatology, and the application of this work to the disposal of radioactive waste gases into the atmosphere. The research is technically administered and supervised through the Air Resources Environmental Laboratory of the Air Resources Laboratories. The work is performed at the Air Resources Laboratories Headquarters in Silver Spring, Maryland, and at the Air Resources Idaho Falls Laboratory, National Reactor Testing Station, Idaho. Any inquiry on the research being performed should be directed to the editor, Isaac Van der Hoven, Chief, Air Resources Environmental Laboratory, Air Resources Laboratories, Environmental Science Services Administration, 8060 - 13th Street, Silver Spring, Maryland 20910.

Table of Contents

ATMOSPHERIC TRANSPORT AND DIFFUSION IN THE PLANETARY BOUNDARY LAYER

AIR RESOURCES LABORATORIES SEMIANNUAL RESEARCH PROGRAM REVIEW
FOR THE ENVIRONMENTAL AND SANITARY ENGINEERING BRANCH
DIVISION OF REACTOR DEVELOPMENT AND TECHNOLOGY
U. S. ATOMIC ENERGY COMMISSION

JANUARY - JUNE 1969

1. RESEARCH AT AIR RESOURCES LABORATORIES HEADQUARTERS, SILVER SPRING, MD.

1.1 Mesoscale Lagrangian Studies (Tetroon Research)

This is a joint research effort of several of the Air Resources Laboratories with the sponsorship of both the Atomic Energy Commission (AEC) and the National Air Pollution Control Administration (NAPCA).

1.1.1 Lagrangian-Eulerian Relationships

A cooperative program between the Air Resources Laboratories, Las Vegas, Nevada, and the Air Resources Trajectory Laboratory, Silver Spring , Maryland, was carried out May 27 through June 4, 1968. Forty-two tetroon flights were made, and high resolution anemometer and bi-directional wind vane data, together with temperature profiles, were obtained from the 1500-ft BREN tower at the AEC Nevada Test Site in Jackass Flats. The purpose of the experiments was to further examine the relationship between fixed point wind data (Eulerian) from the tower and winds obtained in a coordinate system moving with the wind (Lagrangian) as approximated by the tetroon flights. The tower analog data have been successfully converted to three dimensional wind components on computer compatible magnetic tape (67 hr of record at 4-sec intervals, approximately 60,000 data points). During the day clear-cut spectral peaks were obtained from both sets of data. The ratio of Lagrangian period to Eulerian period (β) was computed to average about 2. Before sunrise there is much noise at the high frequency end of the Lagrangian (tetroon) spectrum making the delineation of the spectral peak difficult. For this reason the variation of β with turbulence intensity and lapse rate may not be well defined from this experiment.

1.1.2 Urban Wind Structure Studies - Columbus, Ohio

The capabilities of several of the Air Resources Laboratories (ARL) were combined in a cooperative study of the meteorological structure over the urban areas of Columbus, Ohio, particularly during the night hours. The ARL Division of Meteorology (NAPCA) made simultaneous multiple wind profile measurements across the city with vertical temperature profiles from tethered sondes and helicopter flights, net radiation measurements, airborne infrared temperature scans, surface temperature profiles from automobiles, fixed point wind measurements, and air quality and tracer studies.

These extensive data were supplemented by 80 tetroon flights from March 11 to 23, 1969. Flights were launched from more than 15 different locations around the periphery of the city selected to bring the tetroon trajectory across the built-up areas of Columbus. Flights were ballasted to float as low as feasible, and many flights averaged 300 ft or less above the city.

The experiment provides the first opportunity to test the newly acquired long distance mobility of the M-33 radar system of the ARL Field Research Office at the National Reactor Testing Station (NRTS) in Idaho. The radar with its self-contained power supply was transported to Columbus and operated without incident or interference with electronic functioning. (It has been driven back to NRTS and returned to on-site studies, again without problems.)

This was also the first full-scale experiment using the modernized data acquisition system. Previously it had been necessary to determine tetroon positions by reading three separate and constantly moving dials. The most rapid sustained rate of data readout by this method has been one set each 30 sec , and this rate is difficult to maintain for flights of 6 to 8 hr. Human errors, lack of simultaneity in range, azimuth, and elevation, and variability in successive time intervals degrade data. The effect of these errors has been minimized by statistical smoothing techniques but at the cost of resolution in the high frequency variability of the wind. The new data system simultaneously senses and records the voltages representing range, azimuth, and elevation, transcribes them on computer compatible magnetic tape, and also provides a real time digital record for in-flight analysis and data backup. Sampling rates of 1 per sec are available, but a slower rate of one data set per 10 sec was determined adequate for the Columbus experiment. The data system improves accuracies several fold over the human operator and permits useful real-time data analysis and experiment modifications. Additional benefit is the much more rapid processing of the data for research analyses. Preliminary data reduction, screening and editing, and final statistical analyses of the positions, wind components, cross correlations, etc., plus computer produced plots of the tetroon paths and heights were completed by the Field Research Office staff using the NRTS computer facilities within a few weeks.

Figures 1 and 2 show the computer produced plots of height vs distance for two of the tetroon flights. Figure 1 is for Flight No. 7, one of the few day time flights. The typical large daytime vertical motions with relatively long periods (about 30 min) are evident. The mean height of this flight was 925 m above sea level or about 600 m above the terrain. Figure 2 shows Flight No. 23 between 2200 and midnight. The reduced vertical motion, with oscillations primarily at higher frequencies, is characteristic of the stable lower atmosphere. Flight 23 was much lower, with its average height above ground only 30 m.

The tetroon data and the wind and stability profiles will be analyzed to determine the variations in the components of the wind, especially the vertical wind, as the tetroon moves from open rural areas to sections of the city with an increasing density of buildings and self-generated heat output.

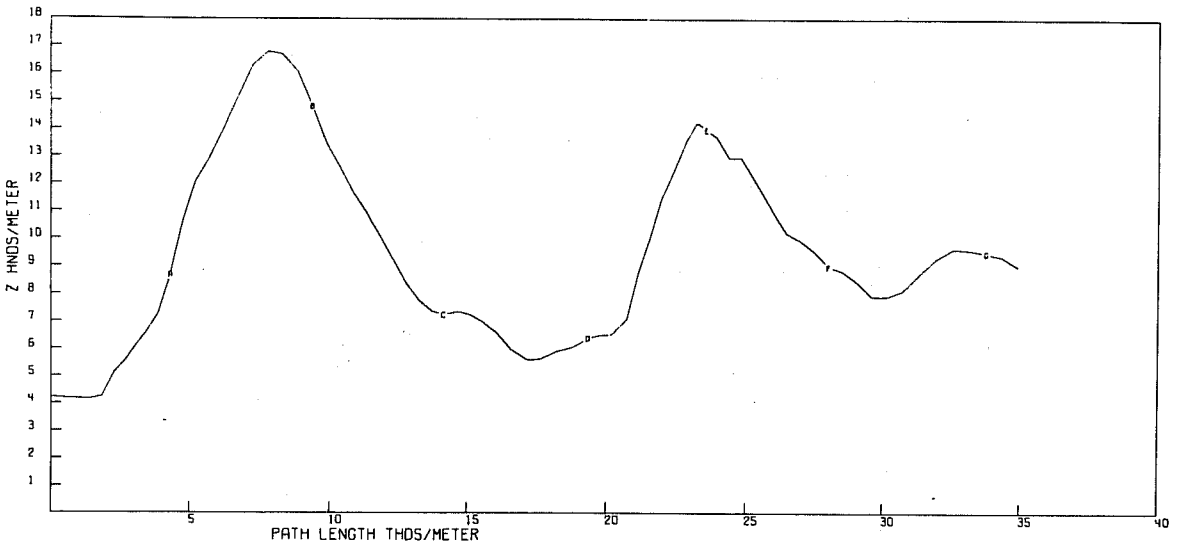

Figure 1. Plot of height versus distance for Flight No. 7 over Columbus, Ohio, on 3/13/69 for period 1445 - 1557 EDT. Letters on curve indicate 10-min periods.

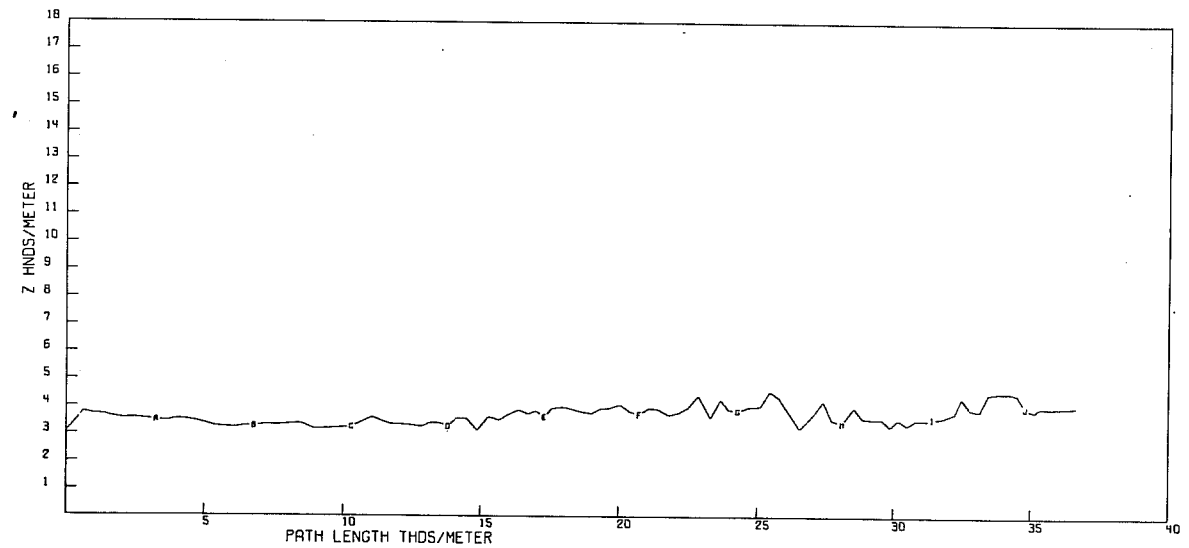

Figure 2. Plot of height versus distance for Flight No. 23 over Columbus, Ohio, on 3/15/69 for period 2211 - 2357 EDT. Letters on curve indicate 10-min periods.

These data can also be used in an entirely different manner. One of the problems in the determination of the transport of pollution over long distances or at heights much above the ground is the absence of frequent upper-air wind measurements. Routine upper-air measurements are made at 6 or 12 hr intervals at widely separated points. Even these observations pass through the layer being measured in only 1 or 2 min, thus providing a very short sample time. Surface wind data, while more numerous, are unrepresentative in both direction and speed of the higher elevations, particularly when the lower atmosphere is stable. It is theoretically possible, however, to calculate the free air or geostrophic wind speed from surface pressure data. The tetroon flights at Columbus, although not designed to test this procedure (they were not designed to float high enough to be in the "free" air flow), offer an opportunity to compare the pressure derived winds with wind directions and speeds averaged over 30 to 60 min. These comparisons are being made with different sets of pressure data to examine the effects of scale (pressure grids of 360 and 260 km) and methods of pressure reduction (station pressure to sea level pressure).

1.1.3 Urban Wind Structure Study - Los Angeles, California

The success of the Columbus experiment has led to the design of a related study in the very different meteorological regime of the Los Angeles Basin during the minimum inversion height period of fall (smog season). The experiment is planned for September 8 through October 10, 1969. This will again be a joint effort of several laboratories. An additional and unique experiment, the use of a helicopter and instrumentation being built by the ESSA Atmospheric Physics and Chemistry Laboratory to measure oxidant air quality along the path of air parcel as depicted by tetroons, has been designed to take advantage of the radar capabilities. Preliminary arrangements for radar and launch site access, electrical power, radio communications, etc., have been accomplished. Support for this work will again come jointly from NAPCA and the AEC, and the activities are being coordinated with other NAPCA air pollution experiments in the Los Angeles area.

1.2 Mixing Length Hypotheses

A modified mixing-length model described previously (ESSA Tech. Memo. ERLTM-ARL 9, 1968) neglects the contribution of a property S to the turbulent flux which arises from the covariance of Δu_i and ΔS and which represents the changes in u_i and S experienced by a fluid particle as it traverses the mixing path. This is equivalent to assuming no correlation between the material derivatives du_i/dt. When measurements were made at a fixed point, values of the material derivatives were not available; therefore, an attempt was made to verify this assumption by examining the correlation between the local derivatives of u_i and S. It now appears that the assumption cannot be tested in this way. Because of the neglect of the advective terms, the local derivative is too poor an approximation to the material derivative. Consequently, in the absence of small scale Lagrangian measurements (i.e., measurements following individual fluid particles), there does not appear to be any way to test this assumption directly. An attempt is now being made to apply indirect tests (i.e., to see whether the expression resulting from neglect of this term is inconsistent with experimental measurements of the turbulent fluxes).

2. RESEARCH AT NATIONAL REACTOR TESTING STATION, IDAHO

2.1 Some Processes Affecting the Transfer of Radioiodine Gas from Air to Grass

This research is jointly sponsored by the AEC Divisions of Reactor Development and Technology and of Biology and Medicine.

Data from 18 field releases of radioiodine gas and environmental chamber experiments collected for the Controlled Environmental Radioiodine Tests (CERT) project were used to summarize our knowledge of transfer mechanisms for elemental radioiodine gas. The processes considered were stomatal transfer, grass leaf cuticle adsorption with dew and humidity effects, surface sublayer transport, and surface boundary layer transport. The surface sublayer is defined as the air layer within the grass canopy, and the surface boundary layer is defined as the lowest few meters above the grass canopy. Details of data collection and reduction are given in previously published progress reports (Markee 1968 and 1969).

The "resistance approach" was used to describe the effect of each contributor to the total adsorption. The total resistance is defined as the concentration of gas in air at a standard height divided by the flux of gas across the surface boundary (grass). Measurements of time integrated air concentration of radioiodine at the one meter level and of total radioiodine absorbed by grass per unit plane area were used to determine the total resistance. The partial resistance of each contributor to the total was then considered in a simple additive manner,

$$r_M = r_{BL} + r_{SS} + r_S,$$

where r_M is the measured total resistance, r_{BL} is the surface boundary layer resistance, r_{SS} is the surface sublayer resistance, and r_S is the surface resistance.

The surface boundary layer resistance, r_{BL}, was formulated by using momentum transfer resistance derived from average wind velocity profiles over the grass during each test. Assuming that thermal energy has a negligible effect in the lowest meter of the atmosphere, the momentum transfer resistance is $\bar{U}/U^{*2}$, where $\bar{U}$ is the average wind velocity at the reference level of one meter and U^* is the friction velocity.

The surface sublayer resistance is a function of leaf surface area. This functional relationship was evaluated for two of the field releases that had a sufficient number of individual measurements of the parameters. The relationships were $r_{SS} \propto A^{-0.80}$ and $r_{SS} \propto A^{-0.73}$, where A is the ratio of leaf surface area to plane surface area. Also an independent check of this functional relationship was made from measurements of profiles of adsorption and of leaf surface area during four field releases. An effective grass

surface area ratio was defined from the profile measurements as

$$EGSA = \frac{A(100 - \sum_i |RA_i - \overline{RA}|)}{100},$$

where RA is the percentage of the total adsorption per unit plane area on a leaf surface area basis for a given height increment of greas. The relationship $EGSA \propto A^{0.75}$ was found for $A < 10$. For $A > 10$, EGSA decreases as A increases; therefore it was assumed that $r_{SS} \propto A^{-0.75}$ for $A < 10$.

The combined effect of r_{BL} and r_{SS} and evaluation of r_S was found for the field data by assuming an equation of the form

$$U^*(r_M - r_{BL}) = \frac{a}{A^{0.75}} + b,$$

where $a/A^{0.75} = U^* r_{SS}$ and $b = U^* r_S$ in which the presumed constants a and b were evaluated by the statistical method of least squares. The statistically fitted line for data collected during unstable conditions (fig. 3) yielded the regression equation

$$U^*(r_M + r_{BL}) = \frac{70.5}{A^{0.75}} + 5.5.$$

Data for stable conditions were scattered widely about this line. The constant 5.5 is most likely indicative of $U^* r_S$ for conditions when the leaf surface is dry and the stomata are closed.

The effects of stomata transfer, dew, and humidity on the adsorption of elemental radioiodine gas on grass were studied in an environmental chamber. Small dimensions and uncontrollable turbulence in the chamber do not permit the determination of surface resistances directly; however, some idea of the magnitude of these effects can be surmised, and the results will be mentioned briefly. With fully open stomata the adsorption was found to be about 2.5 times the value of that with closed stomata. The presence of dew on the leaf surface with closed stomata increased the adsorption by a factor of 1.4. High to low relative humidity adsorption ratios were 1.3 for nighttime conditions and 2.3 for daytime conditions. Stomatal measurements were not made during the humidity tests; so it is not known whether stomatal condition was a factor in the results.

Future field and laboratory experiments, in which the structure of turbulence and gas transfer within the grass canopy will be measured, have been planned so the physical relationships between gas and momentum transfer

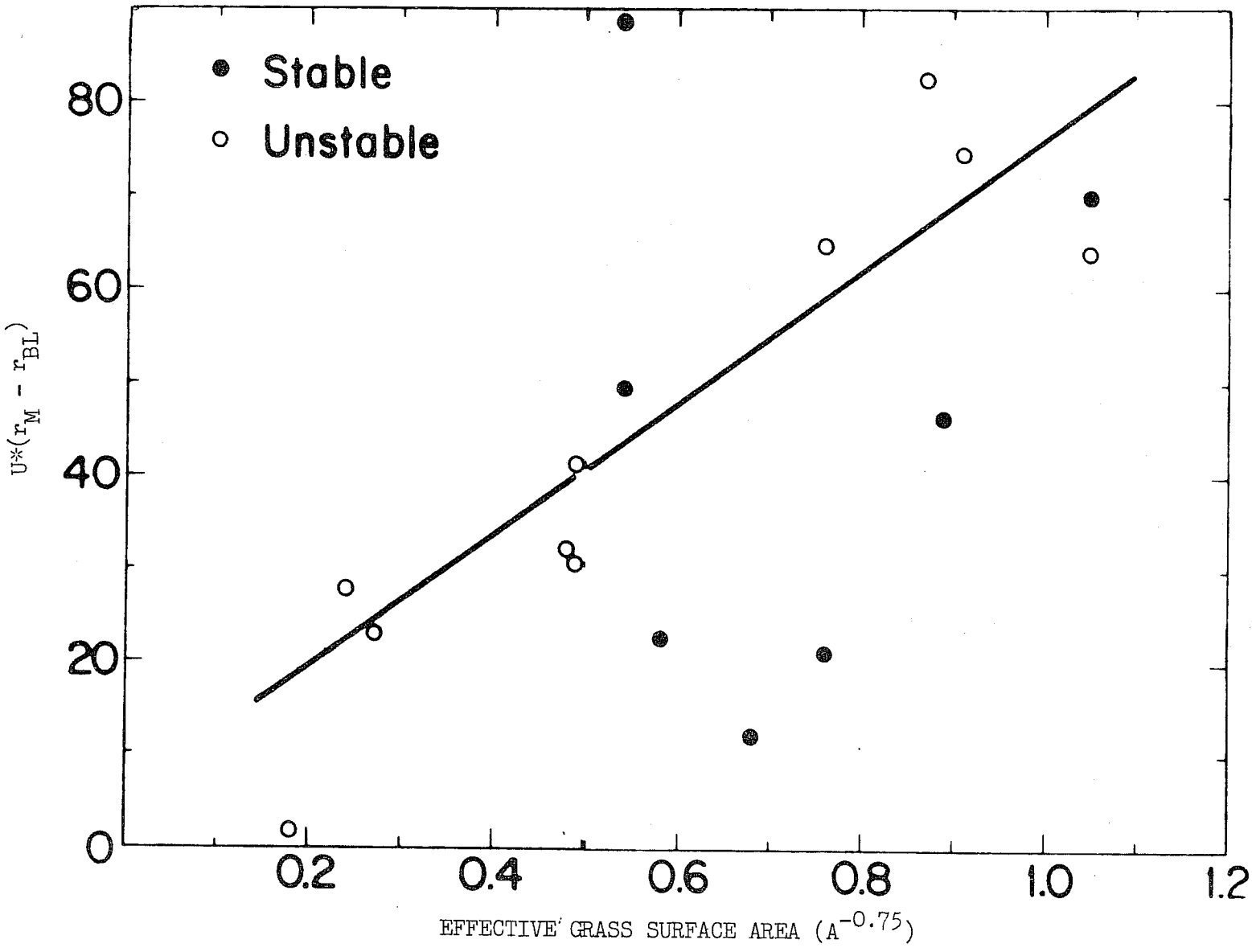

Figure 3. Relationship between $U^{*}(r_M - r_{BL})$ and effective grass surface area (EGSA) ratios.

in the surface sublayer can be studied. Also definitive studies of the effect of stomata on r_s have been planned.

2.2 Mesoscale Wind Field, Transport, and Diffusion Studies

Of the various schemes investigated for the objective interpolation of randomly spaced wind observations to a rectangular grid network, a scheme which uses the average of the station values, weighted by the inverse square of their distances from the grid points, was selected (ESSA Tech. Memo. ERLTM-ARL 9, 1968 and ERLTM-ARL 14, 1969). The station selection process in this scheme has been modified to allow more user control of the process and to make it more efficient for other projects that use the interpolated wind fields to provide an advection or transport process.

In the weighted averaging scheme originally utilized, the stations involved in the interpolation for a single grid point were those that fell within a specified radial distance from that grid point. Increasing the specified distance would increase the number of stations used in the interpolation. At each grid point the radius started small and was increased until at least three stations were involved in the averaging. The idea was sound but the procedure was quite inefficient and somewhat inflexible. The latest modification involves, as an initial step, the computation of the distances of all the stations from a given grid point. These distances are then put in ascending order and the first ten stored. The station subscripts are also reordered accordingly, and the first ten are stored for later use. When this process is completed for each point in the rectangular grid, the stored results are then valid for any number of sets of simultaneous wind data from the network of stations.

As each set of wind observations becomes available, the string of station distances and station subscripts for each grid point are used to determine the closest minimum number of stations, N, for which data are available and whether or not there are more than N stations within a specified radius of the grid point. The minimum number of stations, N, and the limiting radius are specified by the user according to the spacing and density of his data network. For the analyses presented in this report, $N = 3$, and the limiting radius is 2 grid units. This makes a minimum of three and a maximum of six stations in any given interpolation.

Another modification of the wind field computational scheme was the addition of an option to adjust the wind speeds to a common height above the ground. This was done by using the climatological logarithmic wind profile from two locations in the grid (Yansky et al. 1966) Spot checks indicated that this procedure is not valid under very stable temperature lapse rates, but otherwise is quite reasonable.

Considerable progress has been made in organizing the data from the network in a form suitable for efficient handling and analysis. Wind data is now available for 21 separate locations in the Upper Snake River Plain. At

three of these locations, wind and temperature data are available at two levels, providing the opportunity to examine thermal stability along with the wind field analyses. All of this information is now stored on magnetic tape.

One of the important uses for this data at the National Reactor Testing Station is the establishment of a climatology of the transport of effluent from various release locations. With the new data format and some modifications in the hypothetical trajectory construction scheme (ESSA Tech. Memo ERLTM-ARL 14, 1969) work is now proceeding in this area: The first approach to the problem is to simulate the release of hypothetical particles from a selected location, one hour apart, for a period of 12 hours. Each particle is then carried by the wind analyses from the wind stations for a period extending 12 hours beyond the release of the last particle or until it leaves the grid, whichever comes first. The paths of these 12 particles and their hourly positions are then plotted on a diagram containing the site boundaries for geographical reference. A new series of releases is then started one hour after the release of the last of the 12 previous particles and the process is repeated. This means that particles may be released continuously one hour apart during a period of any length for which data are available.

To illustrate the technique a case study covering the period 1300 MST June 28, 1969, to 1200 MST July 1, 1969, is presented. The area of interest for the mesoscale wind analysis is shown in figure 4. The description of these wind fields would be pointless without an understanding of the synoptic scale weather patterns which dominate the surface flows.

The 500 mb analysis began on June 28th with a low pressure center over central Washington at 0500 MST, which progressed rapidly eastward to NE Montana by 0500 MST on the 29th. The 500 mb trough at 0500 MST on June 29th trailed from the low center back to NE Oregon and moved rapidly eastward to the central Rockies as a trough of negligible amplitude by 0500 MST June 30. The movement of the 500 mb low on June 28th and the trailing trough on the 29th triggered light and scattered shower conditions both afternoons in SE Idaho, in spite of the presence of high pressure throughout the period of the study on the surface analysis to the west and north of the area of interest. The 500 mb jet stream was south of the Idaho-Utah border on June 28th and 29th and slowly broadened over the entire area from northern Utah to the Canadian border with speeds of 35 knots from 250° over SE Idaho by 0500 MST July 1. The 500 mb winds over the upper Snake River Plain were 250° to 270°, 30 to 40 knots on June 28th through the 30th except to shift to the 280° to 290° range with the upper air trough passage on the afternoon of the 29th.

Wind field analyses separated by 5 hours from the beginning of the period through 1800 MST, 30 June 1969 in figures 5 (a) through (p). The spacing between grid points is 5.33 miles in these figures. A vector length of one grid unit corresponds to a speed of 25 miles per hour. The wind speeds indicated by the standard wind symbols represent an average wind over a period of an hour. The letter 0 appearing by itself on a plot indicates a station

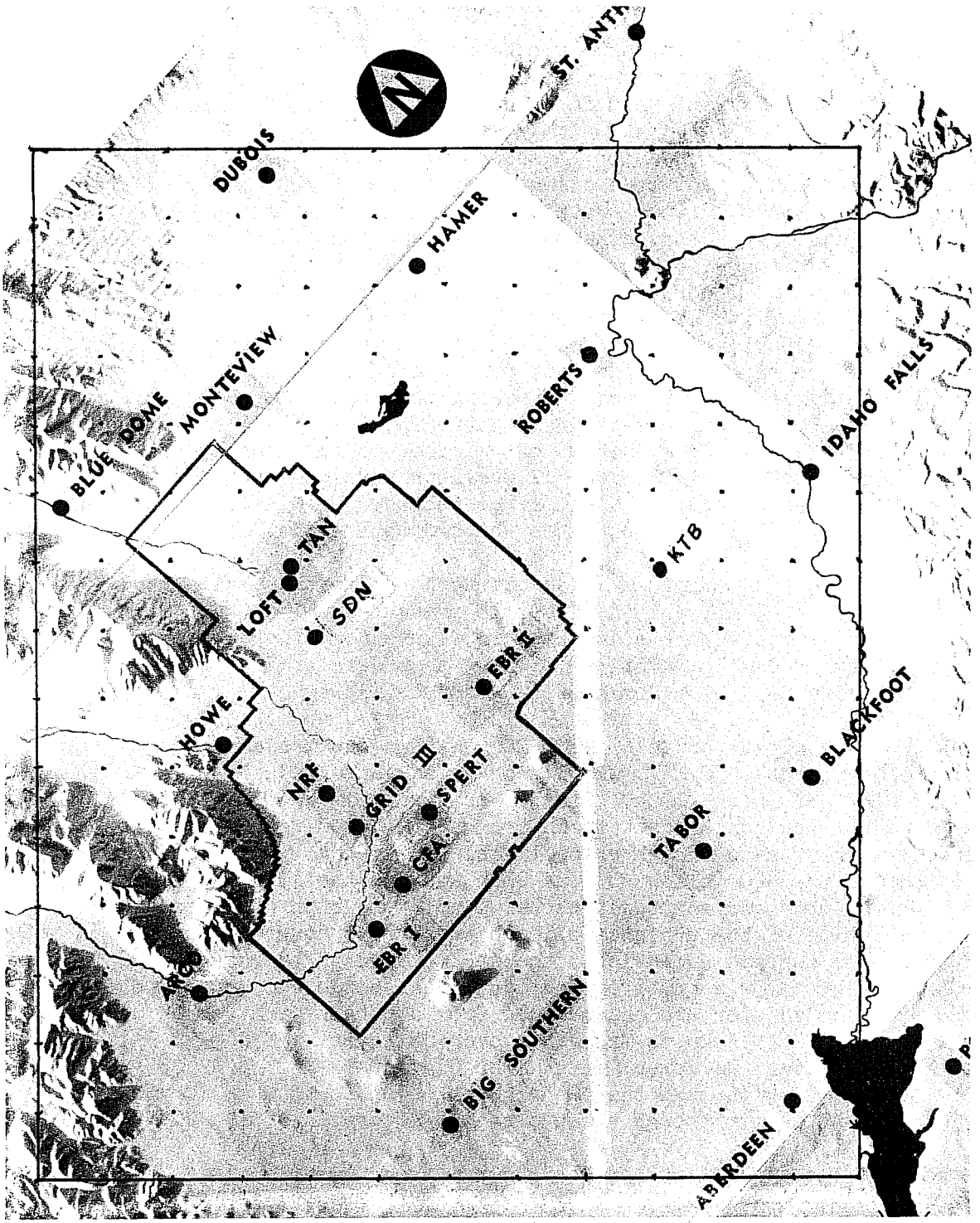

Figure 4. The geographical area covered by the computational grid. The separation of the grid points is 5.33 miles.

location with missing data. The letter O with a wind symbol extending from the center indicates that the wind from that station has been reported to be varying more 90° in direction during the one hour averaging interval. The rectangular grid has been rotated from north in a clockwise direction.

In examining the wind fields in figure 5 (a) through (p) we may note that on the morning of June 28th a moderate southwesterly flow occurs over most of the area, with an episode of strong westerly winds occurring during the afternoon across the southern portion of the site. By 2100 MST (c), the winds on the left half of the grid have become northeasterly, but the winds on the right half remain southwesterly. This condition persists through the night and into the morning hours. By 1200 MST on the 29th (f), the predominantly southwesterly flow has returned and another episode of westerly flow occurs in the afternoon. By 2200 MST (h), northeasterly flow occurs predominantly over the whole grid. During the next two days the winds were generally southerly throughout the day and northerly during the night.

The plots of the trajectories of the hypothetical particles released from a reactor area in the southwest portion of the site are shown in figure 6 (a) through (f). The legends for the numbers and letters appear in table 1. We note from figure 6 (a) that particles 1 through 3 begin moving northward and then turn to the east, reflecting the beginning of the first west wind episode, previously mentioned. Particles 4 and 5, however, begin moving east and turn northward indicating the end of the episode around 1800 MST. Particle 6 seems to get trapped in the vortex indicated in figure 5 (d) and (e). The motions of particles 8 through 12 reflect the light and variable winds over the southern part of the site between 2100 MST on June 28th and 1200 MST on June 29th. The next 12 particles released, shown in figure 6 (b), simply mill around in the area of the release point until the wind picks up between 1000 and 1100 MST and begins carrying the particles northward in a group. The second west wind episode begins around 1400 MST and begins carrying the particles eastward. Between 1600 and 1700 MST the winds become northwesterly and drive the particles through a zone of convergence, which shrinks the cluster of particles as it is carried over a small community about 8 mi south of Idaho Falls, Idaho. The first two particles of the next 12 hour release, shown in figure 6 (c), are carried over a similar path indicating that the same pattern held up until around 1500 MST. From 1500 to 2000 MST the changing flow pattern seems to spray the particles uniformly from an easterly direction through a southwesterly direction. The last 4 trajectories of figure 6 (c) and the first 8 trajectories of figure 6 (d) indicate a fairly steady northeasterly flow from 2000 MST on the 29th through 0800 MST on the 30th. The rest of the trajectories in figure 6 (d) and those of figures 6 (e) and 6 (f) show the characteristics of three reversals between the northerly and southerly flows.

As was mentioned, this 4-day case study is presented primarily to illustrate the tools and techniques under development for the purpose of gaining knowledge of the mesoscale wind patterns and associated transport. However, interesting and unexpected phenomena appear that reveal different aspects of the investigation. These phenomena are the west wind episodes of the afternoons of June 28th and 29th, which seem to be superimposed on the "familiar" cycle of northeast-southwest flow that occurs over this region. A plausible

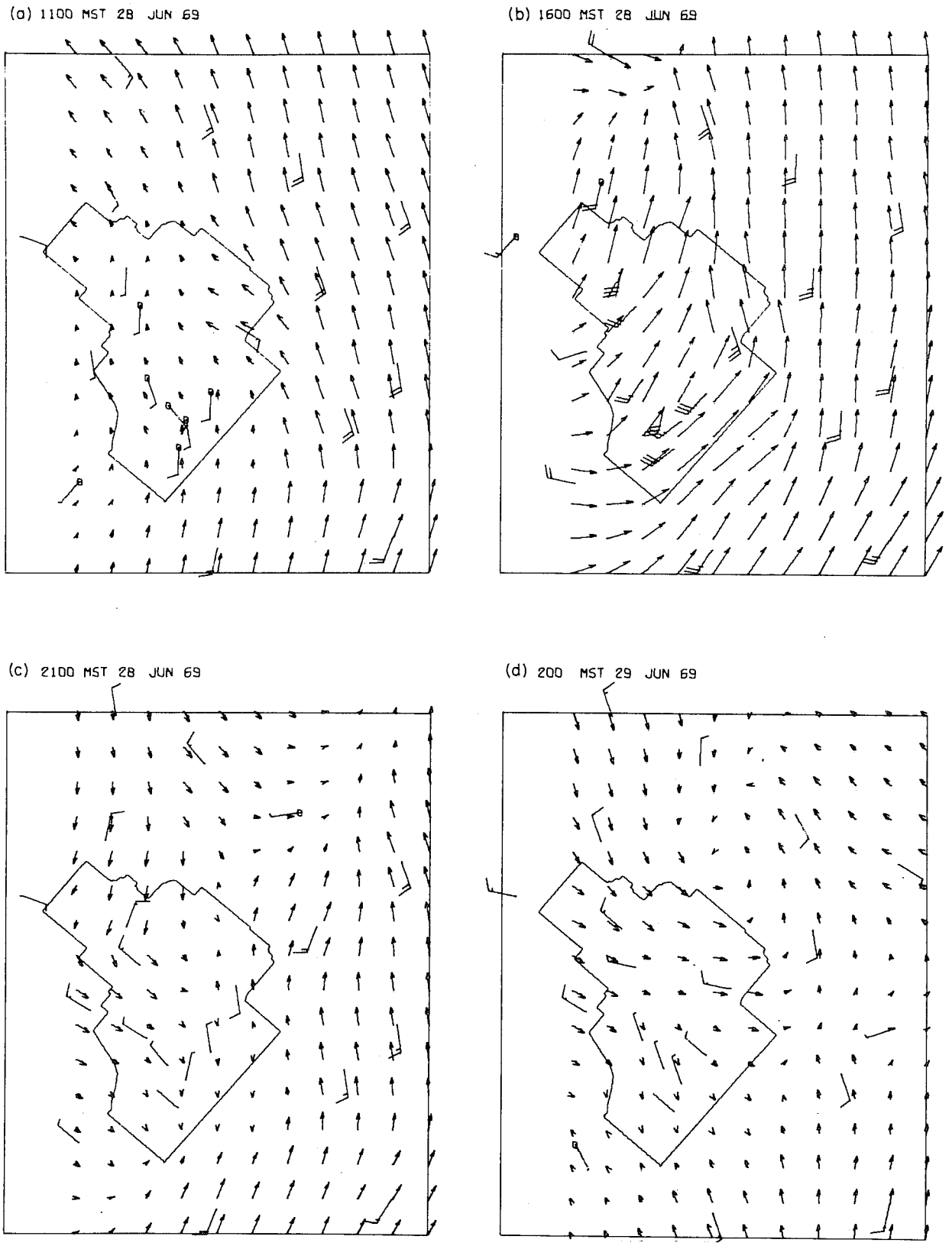

Figure 5. Mesoscale flow patterns depicted by wind vectors obtained by interpolation of hourly averaged winds. A circle at the end of a symbol indicates a variable wind. A circle standing alone indicates missing data.

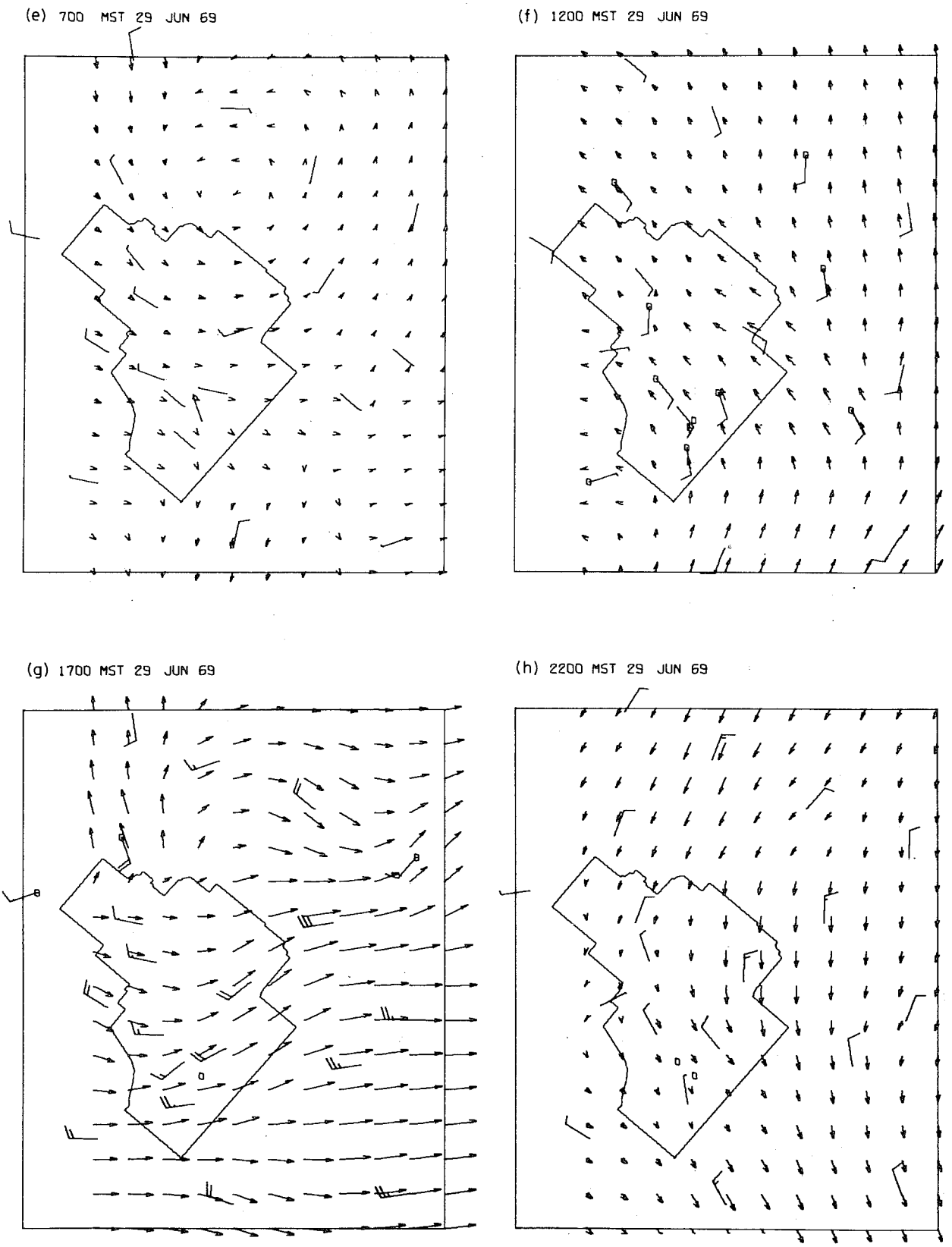

Figure 5. (Mesoscale flow patterns, continued)

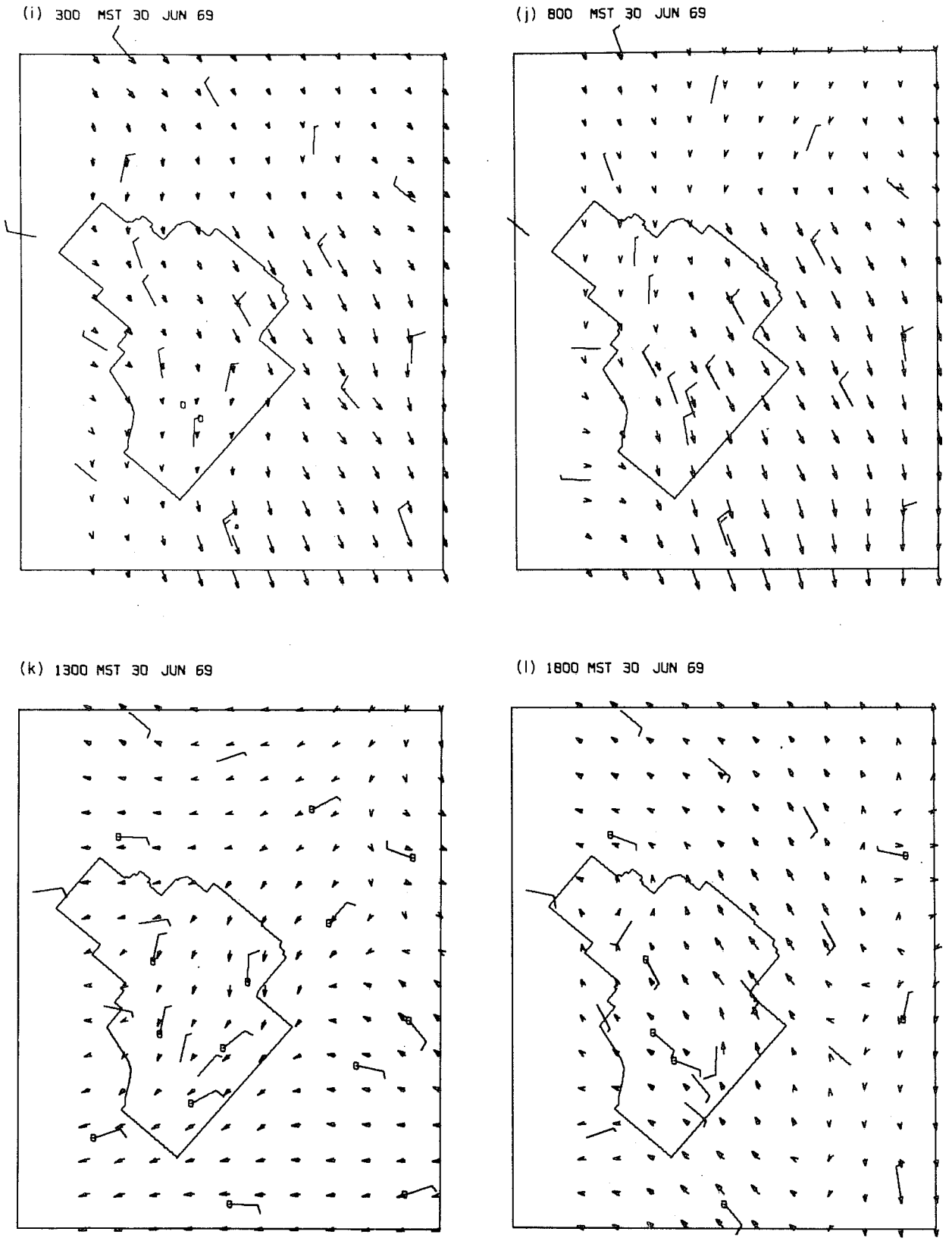

Figure 5. (Mesoscale flow patterns, continued.)

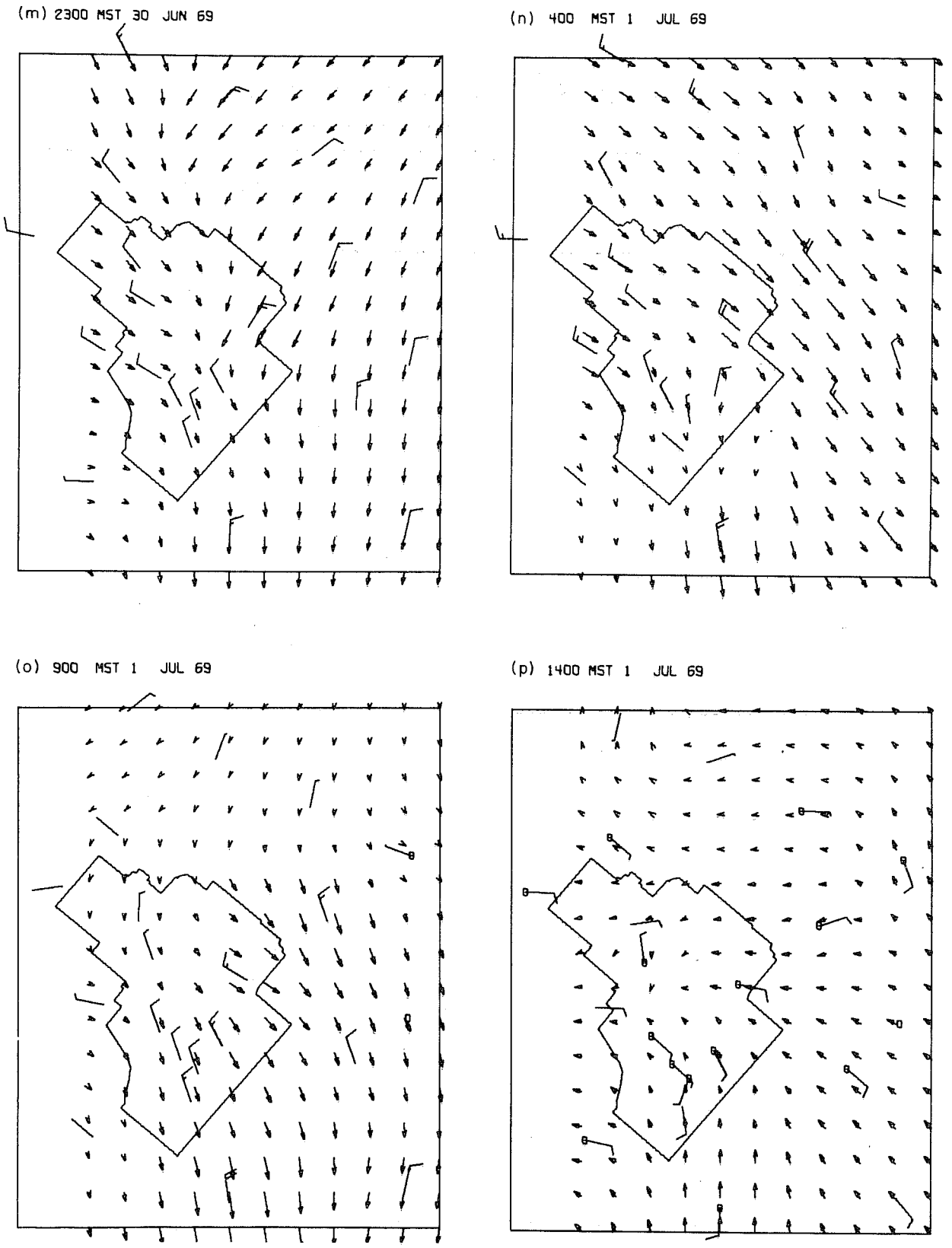

Figure 5. (Mesoscale flow patterns, continued.)

Table 1. Symbols for Particle Trajectories*

Release Duration 0100 - 1200 MST			Release Duration 1300 - 2400 MST		
1		1:00	1		13:00
2	A	2:00	2	A	14:00
3	B	3:00	3	B	15:00
4	C	4:00	4	C	16:00
5	D	5:00	5	D	17:00
6	E	6:00	6	E	18:00
7	F	7:00	7	F	19:00
8	G	8:00	8	G	20:00
9	H	9:00	9	H	21:00
10	I	10:00	10	I	22:00
11	J	11:00	11	J	23:00
12	K	12:00	12	K	24:00
	L	13:00		L	1:00
	M	14:00		M	2:00
	N	15:00		N	3:00
	O	16:00		O	4:00
	P	17:00		P	5:00
	Q	18:00		Q	6:00
	R	19:00		R	7:00
	S	20:00		S	8:00
	T	21:00		T	9:00
	U	22:00		U	10:00
	V	23:00		V	11:00
	W	24:00		W	12:00

* The particle numbers appear opposite their release times. The hourly particle position is indicated by the appropriate letter - time combination.

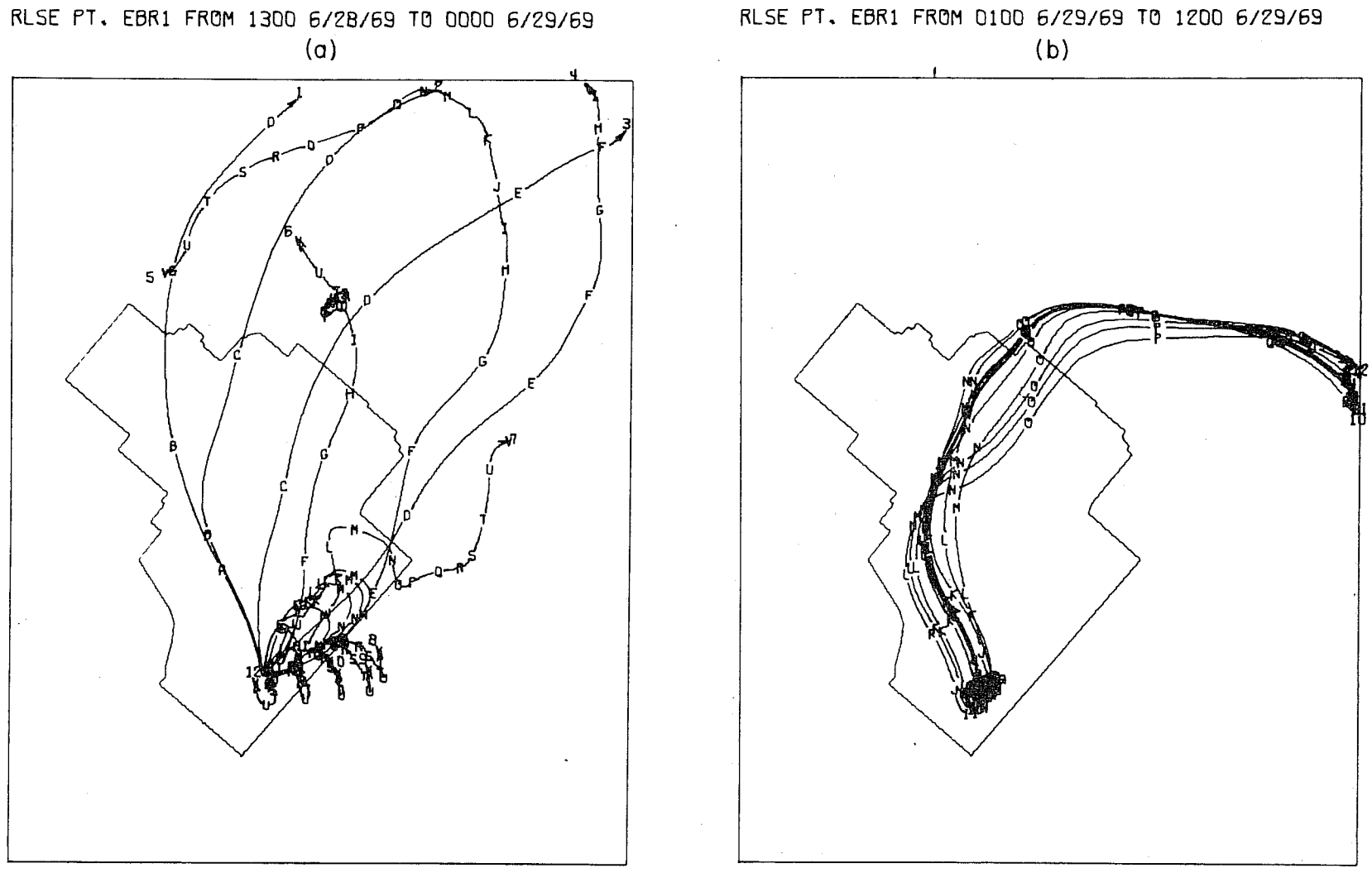

Figure 6. Trajectories of hypothetical particles released hourly and transported by a time series of objectively interpolated wind fields. Particle numbers appear at the end.

RLSE PT. EBR1 FROM 1300 6/29/69 TO 0000 6/30/69

(c)

RLSE PT. EBR1 FROM 0100 6/30/69 TO 1200 6/30/69

(d)

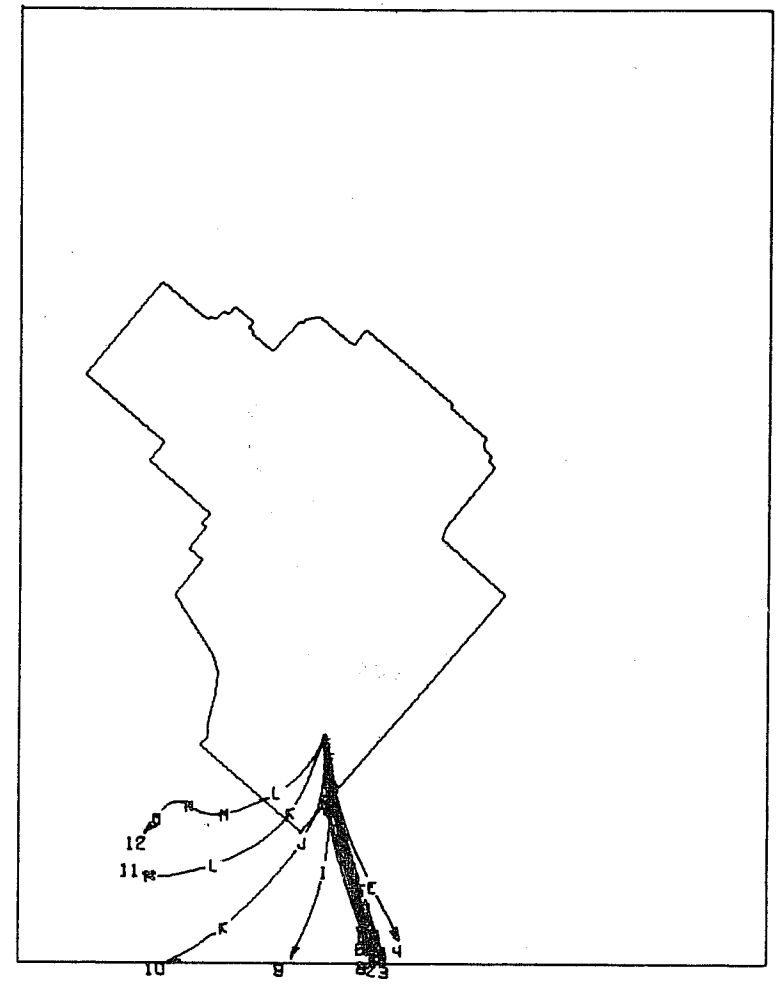

Figure 6. (Trajectories of hypothetical particles, continued.)

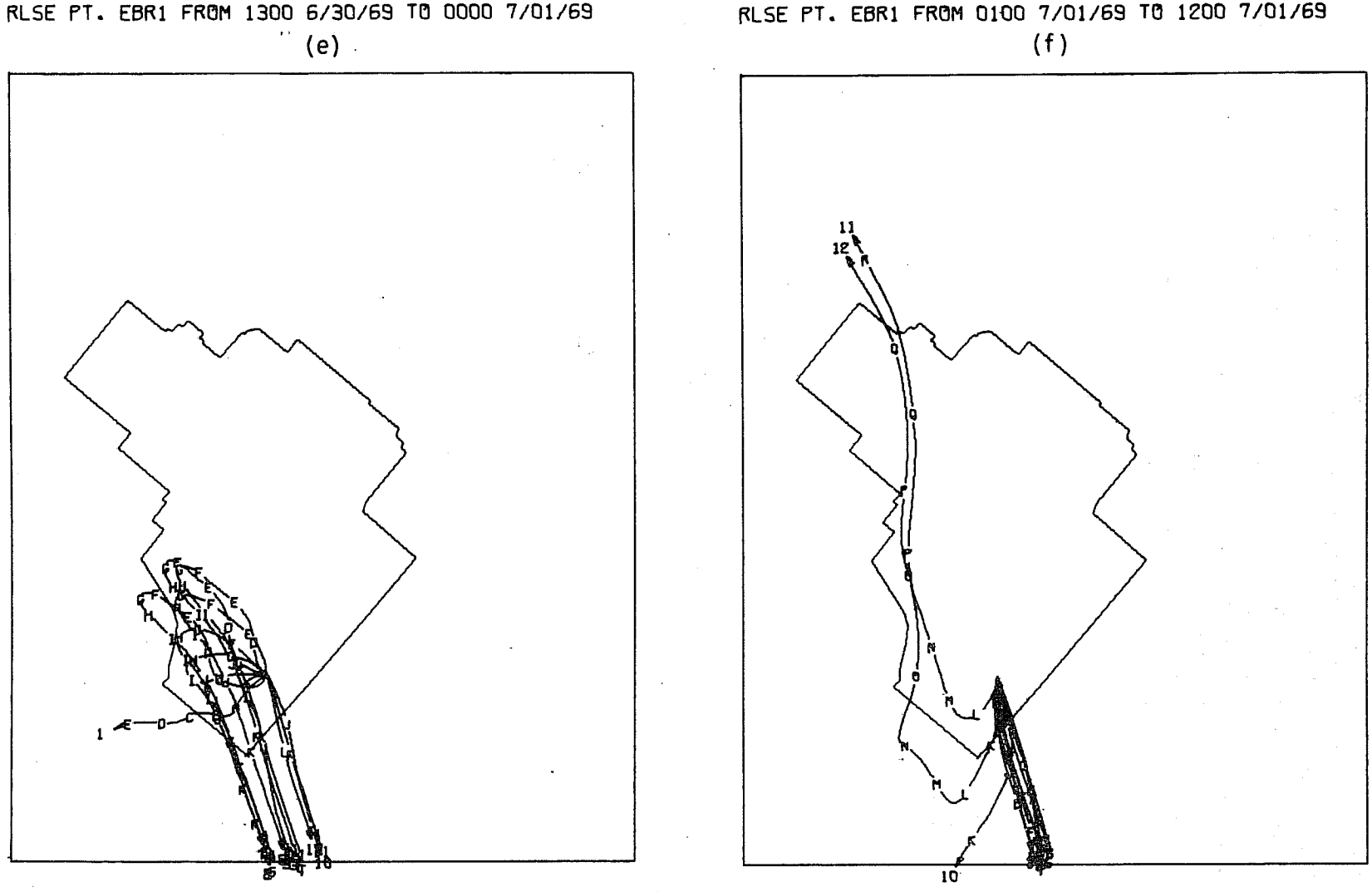

Figure 6. (Trajectories of hypothetical particles, continued.)

explanation for these occurrences seems to be that the strong westerly flow aloft, indicated on 500-mb charts, was transferred downward because of thermal instability (shower activity was noted on both afternoons) and some possible vertical wave activity caused by the mountains to the west. Under certain conditions a knowledge of the upper level large scale flow pattern is critical in interpreting and forecasting mesoscale phenomena. In the case presented here the result of the interaction of the two scales of motion produced a potentially hazardous condition (fig. 6b), which would have been unexplainable from a purely two-dimensional mesoscale point of view of the situation.

There are still many phases of this project in progress, some of which are investigations of terrain effects, the comparison of actual tetroon trajectories with hypothetical trajectories, constructed with the wind field data, the investigation of the validity of the objective interpolation technique, and an attempt to increase the effectiveness of current data collection methods. However, the main effort during this reporting period has been to get the computer programs in operational order. A computational framework has been established that will facilitate, and will itself be improved by, these other areas of research.

2.3 A Statistical Technique for Surface Wind Forecasting

Forecasting of meteorological variables and weather events is dependent on an understanding of meteorological dynamics and physical processes and also on the climatology of the forecast area. Synoptic scale dynamics is the primary concern of other research units with input to the National Meteorological Center for routine dissemination on the facsimile networks. Sub-synoptic and mesoscale dynamics are also the subject of research by a number of units, including the Air Resources Laboratories Field Research Office at Idaho Falls, Idaho, where concern is with mesoscale winds and transport of a pollutant. In the absence of an adequate computer to efficiently handle very small scale and physically realistic mesoscale numerical models and with the lack of a sufficiently dense and accurate network of observations to furnish input to such models, the forecast problem must largely depend on past experiences – statistical meteorology. This section is a status report of four areas of statistical meteorological research at the Idaho Falls office.

2.3.1 Forecast Verification

The complete summary of forecasts of temperature, precipitation and winds over the period February 1965 through June 1969 will appear in the next report. Verification statistics of temperatures, precipitation, and winds are being evaluated on twice daily forecasts, which are issued Monday through Friday except holidays.

The objective in the verification is to find weak points and systematic errors that need further study and to furnish comparative forecasts to evaluate the effectiveness of statistical forecast studies. On data gathered thus far a primary weak point is minimum temperatures in winter. The average

error on 36-hour forecasts of minimum temperatures for the winter months of January, February, and December of the years 1965 through 1969 (except January 1965 and December 1969) is 8.4 degrees F. For the same prediction the average error on 24-hour forecasts is 6.9° and the average 12-hour forecast error is 6.3°.

A systematic error is the forecasting of light northerly winds at night. These forecasts have direction errors in excess of 90°, about 60% of the time. The drainage flow assumption from the north during the night is frequently in error. Northerly drainage flow is more characteristic of early morning hours than hours around and following midnight.

2.3.2 Dependent Data Set Development

Data collection and storage on magnetic tapes for the 7-year period, 1962 through 1968, is nearing completion. This data set will soon consist of the following:

1 Raob tape - 1200 GMT data at mandatory levels up through 500 mbs at Boise, Salt Lake City, Great Falls, Lander, and Winnemucca.

Nine track binary tape with 16 bit words, 62 words per record (one day).

1 Surface tape - 1200 GMT data giving sea level pressure, temperature and wind at Boise, Dillon, Pocatello, and Salt Lake City. Nine track binary tape with 16 bit words, 18 words per record (one day).

12 tapes of D values (one tape for each month) at the NMC grid points. D values available twice daily at 1000, 850, 700, 500, and 300 mbs.

2.3.3 Maps Used

Previous reports have shown the use of map types for predicting precipitation events and maximum average hourly winds in the afternoon. In those experiments, map type predictors explained only 10% to 30% of the variation in winds and 30% to 40% of the variation in precipitation. If many predictors were screened, the map type predictors were selected only when they give significant information not in other predictors. Since map types really represent a two-dimensional field we can only say we have or don't have a given pattern; these are binary variables. The type of predictand determines whether this binary variable can be significant when compared to other variables for prediction. This may well be the case with weather events where spatial distributions of height contours and vorticity (i.e., gradients) may explain more than point values. A problem develops if considerable variation in pattern is allowed for maps within a given type map. Therefore, very high correlations are required for meaningful designation of any given map as a particular type, and a great many map types will be derived.

A primary problem of map types selected through the linear correlation process is the statistical step of dividing data values by the standard deviation of data values for the whole map. This means only pattern counts, not gradients. Two zonal maps are perfectly correlated if the north-south gradients are a constant, even though the gradient on one map is twice the gradient on the other map. This implies that better map types may be found if gradients enter the correlation. Experiments testing the prediction ability of map types with gradients, as compared to those without, have begun.

2.3.4 Wind Studies

Because a primary concern of the laboratory is the small scale transport of pollutants, the primary objective of forecast research is wind prediction, both at a point and in a region. In the absence of prominent terrain or large water bodies the two scales of prediction (large and small) are probably the difference in winds between random points within the mesoscale region.

The study of wind fields in the upper Snake River Valley, where prominent terrain features do influence the mesoscale wind field, is presented in section 2.2 of this report. In addition, the wind fields are being studied from the forecast point of view. They are divided into classes or types of flows, which in turn can be forecast.

An initial attempt at classifying wind fields was the linear correlation technique, where the u and v data points from every pair of wind fields were correlated. The experiments could consist of 'synoptic' wind fields or wind fields involving data points from one or more stations over a period of time. The latter technique was tried with 16 data points per sample case consisting of the u and v components for the eight 3-hourly observations beginning at 0200 MST at the Central Facilities Station of the NRTS. The total sample consisted of 434 days from January, February, and December for the years 1962 through 1966. The first three types are shown in figure 7. It may be noted that these first three types reveal the systematic forecast error on nighttime winds, as mentioned earlier. In winter the winds tend to blow from the SW to W at night. The problem of gradients, as mentioned in the section on map types, was again a bothersome nuisance but in addition the departure from the mean was a problem too. Figure 8 shows two cases correlated at 0.89. If the data points for each case are normalized by subtracting the case mean and dividing by the case standard deviation, the two sets of data points will be very similar. To avoid the problems arising from normalizing data to ordinary linear correlation, another system of "correlation" is being investigated.

A second approach to classifying wind fields was to use a coding technique. The wind rose is divided into classes and the mesoscale wind field to be coded is divided into regions. The code for any given case is the sequence of area regions. An experiment was conducted in which the upper Snake River Valley was divided into three regions, NW, SW, and E. Each region had six wind stations whose recorded winds were averaged to determine

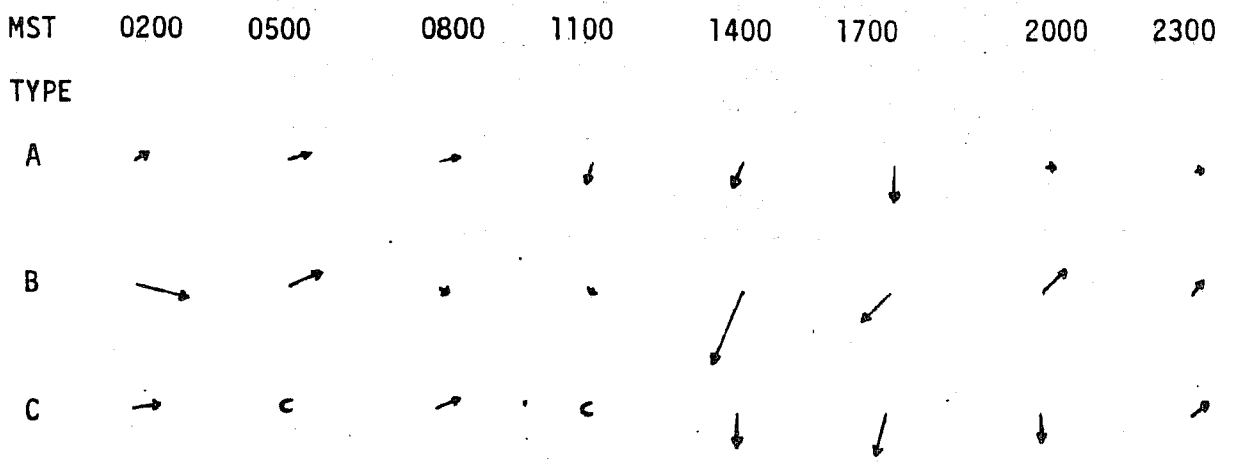

Figure 7. The first three derived daily wind types for winter at CFA. (Wind arrow scale: 1 mm = 1 mph.)

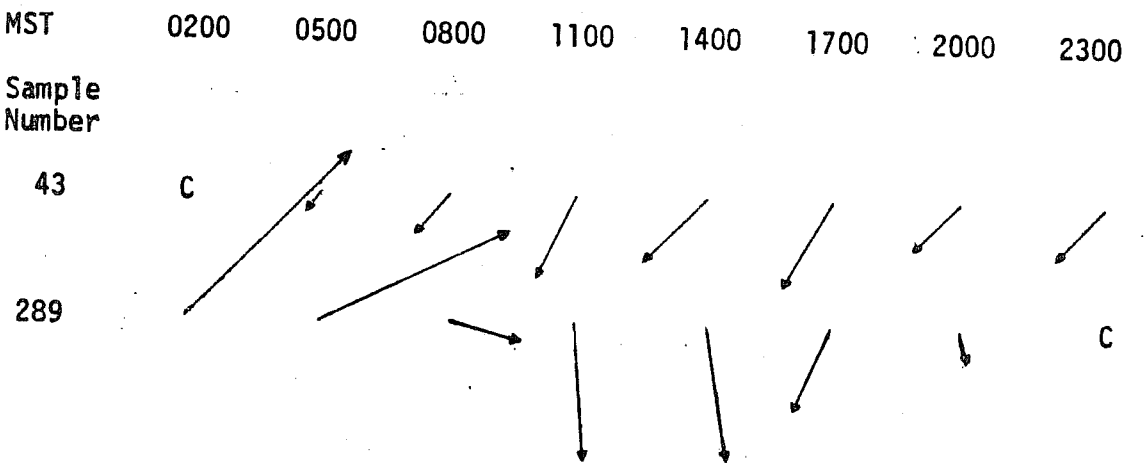

Figure 8. Two sample days correlated to one another at 0.89, chosen to illustrate the effect of normalizing data for linear correlation. If plots of the normalized data were shown the two samples would appear nearly identical.
(Wind arrow scale: 1 mm = 1 mph)

the characteristic wind for that region. The wind rose was divided into eight classes. The experiment consisted of the 672 hours in February 1969, and the 720 hours in June 1969. Even with mere three digit codes there were about 75 different classes in the nearly 1400 cases. Many cases produced spurious coding because of wind shifts within the region. The coded wind was then the result of two opposing wind directions, neither of which was similar to the wind implied by the resultant area code.

Work will continue to test the tentative conclusion that the variety of wind flow patterns in the mesoscale is too great to adapt to 'type' forecasting.

2.3.5 Forecast Techniques

Personal communication with Dr. Harry Glahn (Weather Bureau's Techniques Development Laboratory) revealed that if multiple linear regression is used to predict u and v components at a terminal, the two simultaneous equations maximize the explained variance of the total wind, as well as the explained variance of the individual components. The use of linear regression on the wind components should be superior to the REEP approach.

The problem of usage of qualitative variables was examined for potential processing by linear regression. The correlation between a binary (qualitative) variable and a continuous variable does not have the range of -1 to +1. To find the range, assume (1) continuous variable, $x = X-\bar{X}$, is normally distributed; (2) binary variable, 'Y', has value +1 for all positive 'x' and value '0' for all negative 'x'; and (3) assumptions (1) and (2) form a perfect correlation.

The correlation formula is

$$r_{xy} = \frac{\Sigma xy}{n\sigma_x\sigma_y} .$$

Assumption (2) results in $y = \pm 1/2$, and $\sigma_y = 1/2$,

$$r_{xy} = \frac{1/2\Sigma|X|}{n\sigma_x(1/2)} ,$$

$$r_{xy} = \frac{\Sigma|z_x|}{n} ,$$

where z_x is the normalized variable for x, and

$$r_{xy} = |\bar{z}_x| ,$$

which is the center of gravity of one tail of the normal curve.

The normal curve cumulative frequency function is

$$\int_0^z \frac{1}{\sqrt{2\pi}} \exp(-z^2/2)dz \ .$$

For $z \to \infty$ the integral $\to 1/2$.

Center of gravity in one tail is

$$\frac{\int_0^\infty \frac{z}{\sqrt{2\pi}} \exp(-z^2/2)dz}{1/2} \ .$$

Substitute the variables in the following way:

$$z = au$$

$$z^2 = a^2u^2$$

$$dz = adu$$

$$b\int_0^\infty z \exp(-z^2)dz = \int_0^\infty bau \exp(-a^2u^2)adu = a^2 \int_0^\infty bu \exp(-a^2u^2)du \ .$$

The value of the left hand integral is b/2. Except for the factor a^2, the right hand integral is the numerator we wish to evaluate. Since $a^2 = 1/2$ and $b = 1/\sqrt{2\pi}$, the center of gravity is $\sqrt{\frac{2}{2\pi}}$. Thus, to make the range of correlation -1 to +1, the correlation between binary and continuous variables would be multiplied by $\frac{1}{.7947}$ or 1.256.

2.4 Turbulence Analysis

In order to examine more closely the true response characteristics of the cup anemometer used in conjunction with bi-directional wind vanes in the analyses of velocity fluctuations (ESSA Tech. Memo ERLTM-ARL-5, 1968) an experiment was conducted to obtain data simultaneously from a cup anemometer and a hot wire anemometer for a comparison of the energy spectra.

The hot wire anemometer was made of Kovar and was .001-in. in diameter and .134 in. in length. The frequency response was reported to be 1000 cps. Because of damage to the array of hot wires in shipment, only the vertical wire was suitable for use in this experiment. For this reason only the horizontal component of the wind was measured. The data from the hot wire were recorded on analog tape to allow sampling rates on the order of 40 readings per second. In the digitization process of the analog data a low pass filter was used to eliminate noise above 40 cps.

The cup anemometer used in the comparison is stated by the manufacturer to have a distance constant of five ft and an accuracy within $\pm 1\%$. The data from the cup anemometer was recorded digitally at a rate of one reading every 2 secs. The data is subjected electronically to a 2-sec averaging before recording. This rate was used because it is a standard rate used by personnel at this office when recording data from 20 sensors on the 200-ft tower.

Both sensors were mounted 2 m above the ground approximately 1 m apart on a line perpendicular to the direction of the mean wind. The data for this comparison were collected in the late afternoon and evening on a clear day in April 1969. Because of technical difficulties encountered in obtaining the data from the analog tapes, the sample for comparison was less than 20 mins in length. This is sufficient to examine the hot wire data, which were digitized at an interval of .026 sec, but a much longer sample should be used for data in which the sampling interval is 2 sec. A much longer sample of the hot wire data will soon be available for analysis. It is felt, however, that the results of the short sample comparison and a look at the energy spectrum for a 4 hr and 33 min sample of cup data are worthy of presentation here.

The period of direct comparison was 1536 MST to 1553 MST, April 3, 1969. The average temperature at 2 m was 51°F. The lapse rate was -3.5°F in 61 m. The average wind and turbulence conditions measured are shown in table 2. We note here that averaging the hot wire data, in order to obtain samples 2 sec apart, has reduced its variance below that of the level of the cup anemometer. However, the variance for the instantaneous hot wire data was about 45% greater than the instantaneous cup data.

Table 2. Wind Statistics

Sensor	Δt sec	$\bar{u}$ (m/sec)	$\overline{u'^2}$ $(m/sec)^2$
Cup Anemometer (Instantaneous values)	2.0	7.2	1.46
Hot Wire Anemometer (Average over 77 points per data value	2.0	7.2	1.33
Hot Wire (instantaneous values)	0.026	7.2	2.11

The normalized energy spectra for the 512 points (17 min 4 sec) of averaged hot wire data and 512 points of the instantaneous cup data were computed and are presented in figure 9. The first ten (10^{-3} to 10^{-2} cps) spectral estimates shown here are unsmoothed and because of the short data sample are of questionable reliability for both sets of data. However, the same general characteristic is demonstrated by both spectra over the entire band presented.For eddies with periods longer than 25 sec (frequency = .04 cps), the data from the cup anemometer (solid curve) indicated a relatively higher energy, and for eddies with periods shorter than 25 sec, the data from the hot wire anemometer (dashed curve) shows a relatively higher energy. In estimating the slope of both spectra it appears that for frequencies higher than .05 cps, the spectra from both the hot wire and the cup data have a slope between -2 and -5/3.

In order to obtain more reliable spectral estimates in the higher frequency range the instantaneous (Δt = .026 sec) hot wire data was divided into five strings of 8192 points each. The normalized energy spectra were computed for each string of data and averaged at each frequency. The result is shown in figure 10. For frequencies higher than .009 cps the hot wire spectral curve from figure 9 (Δt = 2 sec) is superimposed as a dashed line. We may note here that the slope is quite close to -5/3 in the frequency range .1 cps to 3 cps. For frequencies above 3 cps, however, three very distinct peaks occur. The major peak occurs in the neighborhood of 9 cps. These peaks were very consistant in each of the five individual spectra. The means for each string were within 6% of the mean for the whole sample, and the individual variances were within 18% of the variance of the entire sampling.

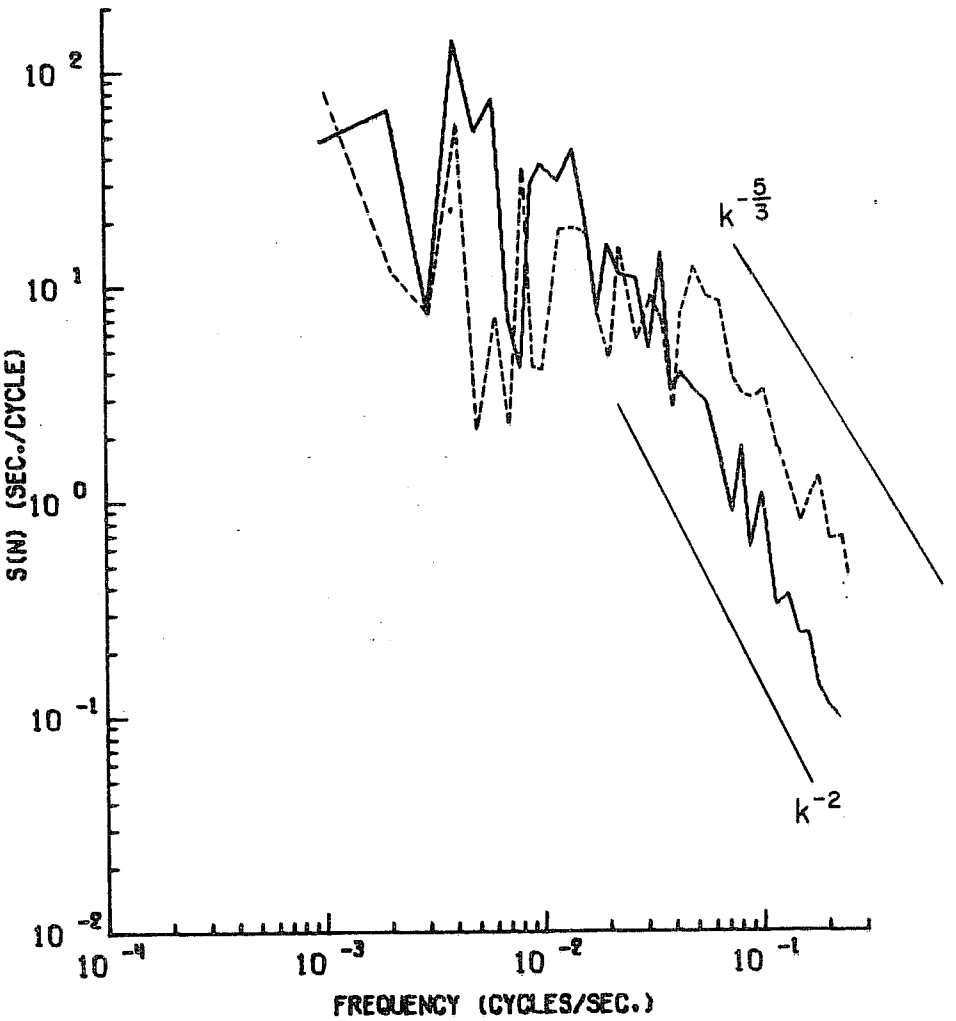

Figure 9. Normalized kinetic energy spectra. The solid curve is derived from the velocity measured by a cup anemometer. The dashed curve is derived from velocity measured by a hot wire anemometer. The duration of the data sample was 17 minutes, 4 seconds. Each discreet data value from each sensor represented a 2 second average. Both anemometers were mounted two meters above the ground.

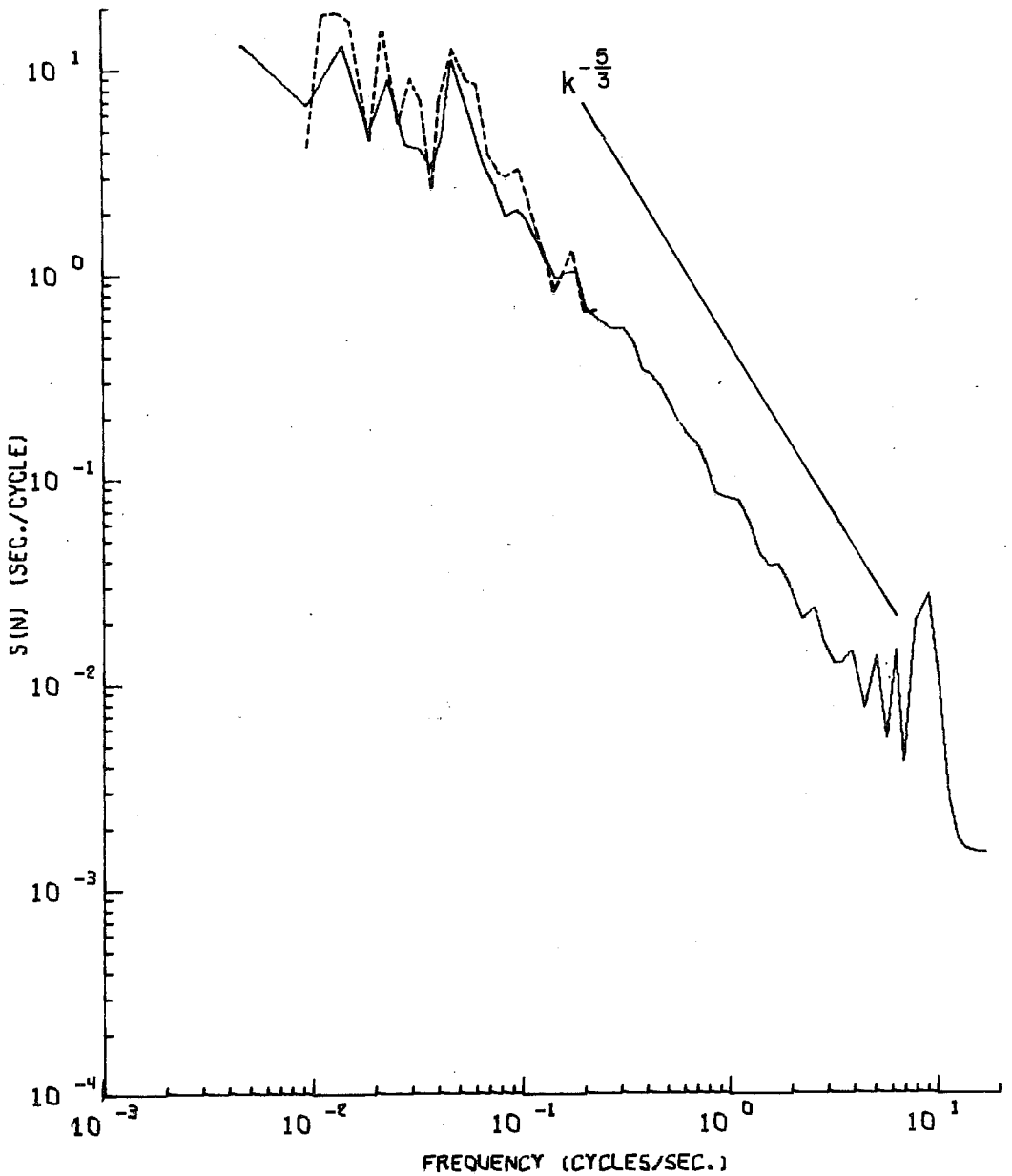

Figure 10. Normalized kinetic energy spectra. The solid curve represents an average of five such spectral curves derived from hot wire anemometer velocity data. The data samples were from five consecutive 3.4 minute samples from the same period as in figure 7. The discreet readings were separated by .026 seconds. The dashed curve is reproduced from figure 9.

In order to get more reliable spectral estimates with the cup anemometer, an energy spectrum was computed for a period of data beginning about 4 hr before the comparison sample and including the comparison sample (8192 points, $\Delta t = 2$ sec). This energy spectrum is shown in figure 11. For frequencies above 0.05 cps the slope is very close to -2. There appears to be a peak in the spectra at a frequency of about .005 cps or a period of about 3.3 min and a minor gap at about .003 cps (5.5-min period).

From this comparison it appears that the combination of cup response and the electronic averaging before recording the data are noticeably affecting the measurement of turbulent activity with periods from 4 to 20 secs. Since the effect is the reverse of what one would expect from aliasing, the cup response might be the most serious contributor. It is interesting to note from the comparison in figure 9 that the straight averaging of 77 points of the analog data to produce a sample with $\Delta t = 2$ sec had no severe effects on the energy spectrum. In order to verify these results, longer concurrent samples need to be obtained. Also the effect of reducing the 2 sec electronic averaging time should be investigated. The distinct peaks in the high frequency end of the spectra of the hot wire data are assumed to indicate a vibration in the shaft used to support the instrument. This problem can be easily remedied by securing the shaft and mount more firmly.

The overall purpose of this type of work is to determine the representativeness with which electronics and mechanical sensors report the turbulent fluctuations of atmospheric phenomena. It is especially essential that this information be available before extensive experimentation and computation be carried out in studies involving the turbulent transport of sensible heat and momentum or in studies of the relationship of turbulence to diffusion. Work is currently in progress in which the response characteristics of a thermocouple are being examined under various configurations of exposure to the atmosphere. It appears that the combination of the electronic computer, high speed recording equipment, and the Fast Fourier Transform Technique have shifted a good portion of the burden of responsibility in the study of atmospheric turbulence back to the sensors.

2.5 Sampling Time Effects on Measurements of Surface Boundary Layer Turbulence

The effects of sampling time on measurements of the orthogonal components of surface boundary layer turbulence were examined for sampling intervals of 1, 3, 6, 9, 15, 30 and 60 min. Eighty-four hours of 2-sec, digitally-sampled bivane and cup anemometer data from the 16-m level of the Grid III tower were used for the analysis. These hourly data were obtained from semicontinuous records collected during the summer of 1968. Most of the data were collected during nighttime conditions. Average values of u'^2, v'^2, w'^2, $\overline{u'w'}$, $\overline{v'w'}$, and $\overline{u'v'}$ were computed for each of the sampling intervals within each 1 hr period. These turbulence parameters were then stratified into atmospheric stability regimes by Richardson number, Ri, (Slade, 1968) calculated from wind speeds and temperature at the 8 and 32 m levels (table 3).

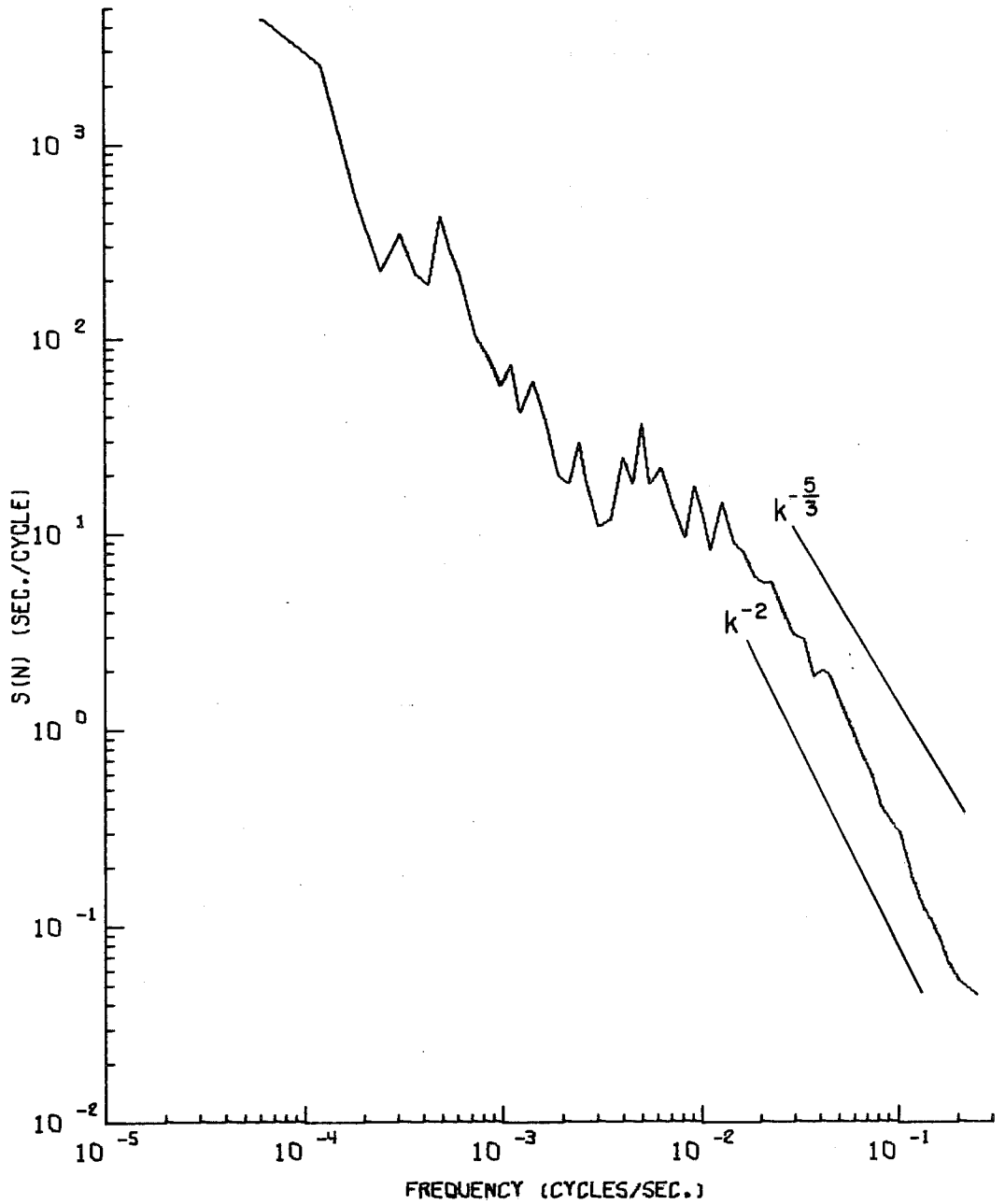

Figure 11. A normalized kinetic energy spectrum obtained from 4 hour and 33 minute sample of velocity measured by a cup anemometer. See figure 9 for details.

Table 3. Atmospheric Stability Regimes

Regime	Ri Range	No. of hrs	Mean Wind Velocity (m/sec)
Strongly Unstable (SU) windless convection	≤ -1.00	16	2.8
Moderately Unstable (MU) free convection	$-1.00 < Ri \leq -0.03$	17	7.0
Moderately Stable (MS) near laminar flow	$0 > Ri > 0.20$	18	4.9
Strongly Stable (SS) induced turbulence episode	≥ 0.20	33	1.7

Average ratios by stability regime of the orthogonal component variances, u'^2, v'^2, and w'^2, for the short sampling intervals to those for the 60-min sampling interval were computed (fig. 12 a through c). Also the average correlations between components were computed by sampling interval and stability regime (fig. 13 a through c). These average relationships summarize the data for this study.

Some of the significant findings from this study follow: The longitudinal (u) and lateral (v) velocity variance ratios show a significantly large variation with sampling interval, while the vertical (w) velocity variance shows only a small variation. Thermally driven turbulence is a separate and distinct contributor to lateral velocity variance during unstable conditions as evidenced by inflection points in the curves (fig. 12 b) between the 6 and 15 min sampling intervals. Undulations in the longitudinal and lateral component velocities produce contributions to their respective variances for sampling intervals greater than 6 min.

The correlation between longitudinal and vertical velocities (fig. 13 a) becomes less negative as the sampling interval is increased. The average u - w correlations during strongly stable conditions are positive for sampling intervals greater than 9 min , which indicates a net upward flux of momentum at low frequencies.

The average crosswind - vertical velocity correlation (fig. 13 b) becomes decreasingly positive for all stability regimes, except the strongly unstable period. During strongly unstable condition, the average correlations are all negative, becoming significantly large negative values at long sampling

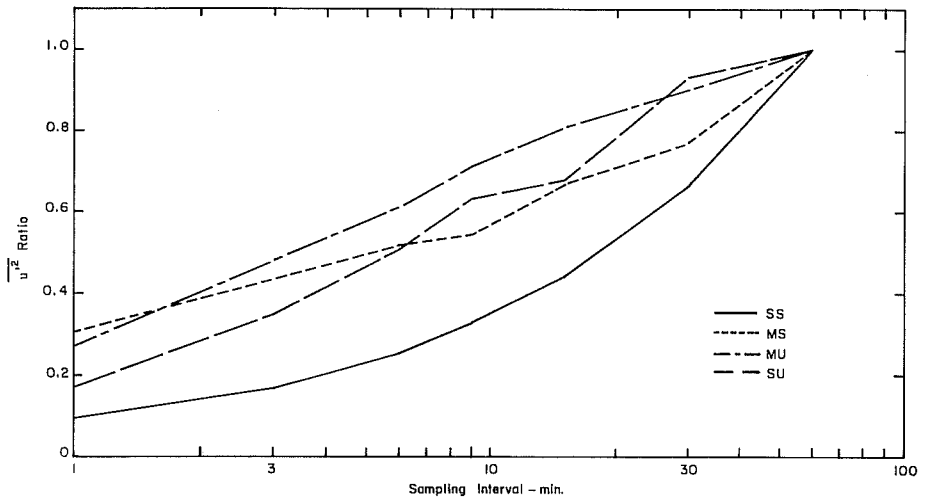

(a)

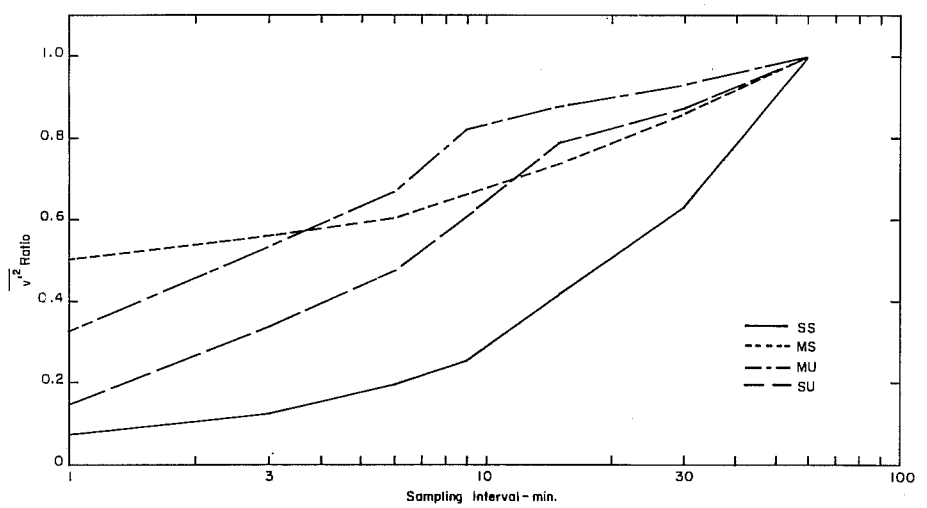

(b)

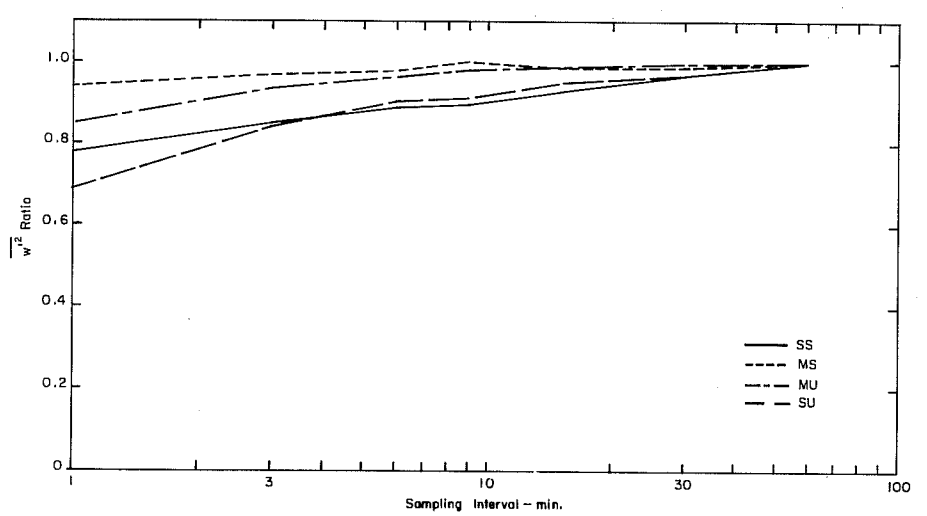

(c)

Figure 12. Variation in mean relative longitudinal (a), lateral (b), and vertical (c) velocity variance with sampling interval as a function of stability regime.

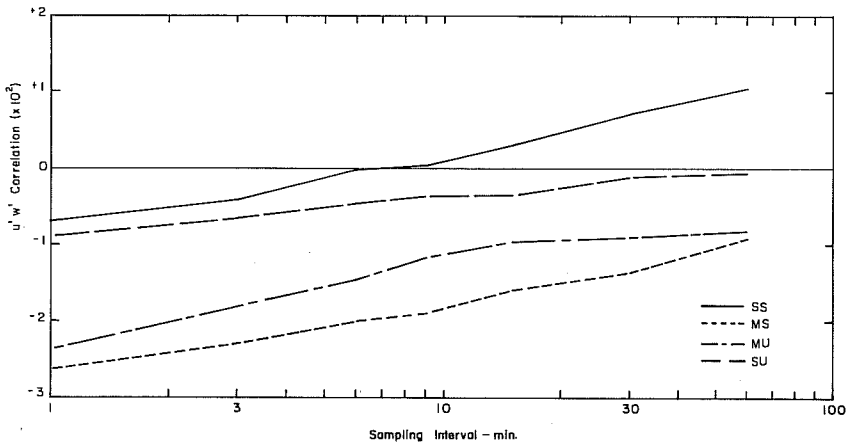

(a)

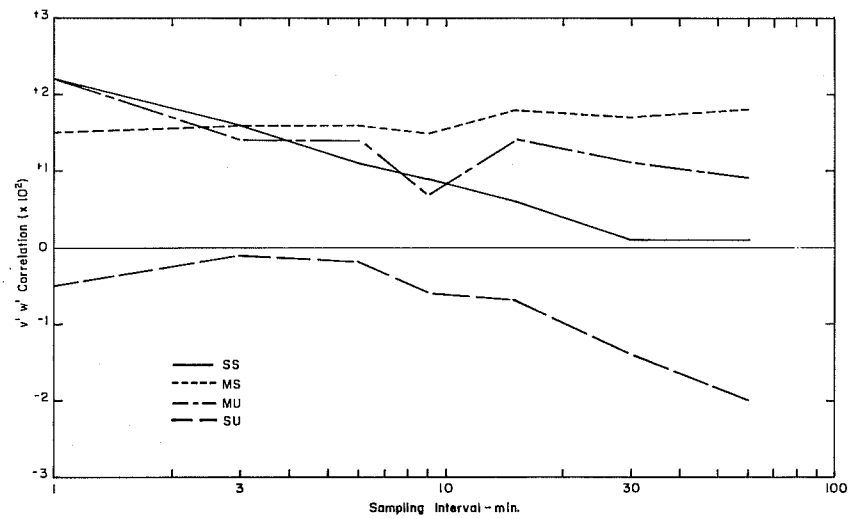

(b)

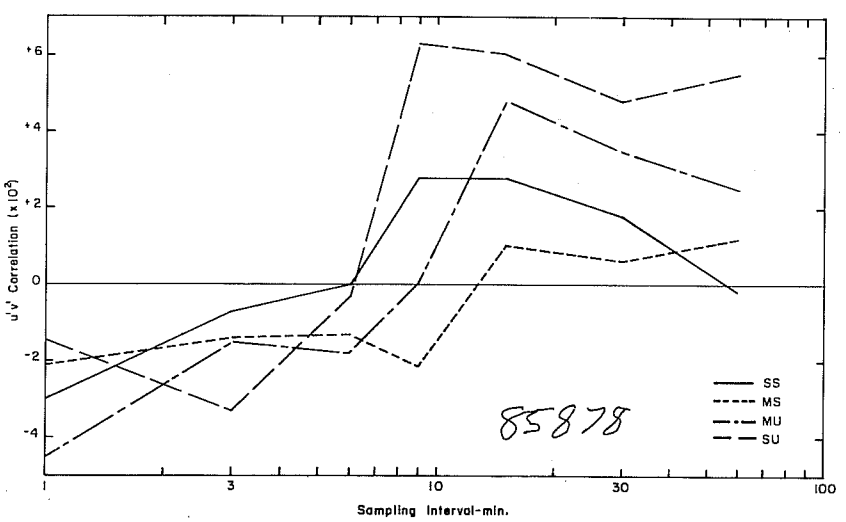

(c)

Figure 13. Variation in mean correlation between u and w (a), v and w (b), and u and v (c) with sampling interval as a function of stability regime.

intervals. The sign of the correlation coefficient determines the direction of the net rotation of the air motion in the crosswind--vertical plane.

In the horizontal plane (u - v plane) the sign of the average correlation coefficients during all stability regimes (fig. 13 c) is negative up to sampling intervals from 6 to 15 min and positive for longer sampling intervals. This result indicates the tendency for helical flow about the mean air flow in a counterclockwise direction at high frequencies and in a clockwise direction at lower frequencies.

In summary, the results of this study show that the selection of sampling interval for turbulence computations is very important. Instantaneous deviations from vector mean velocities determined from sampling intervals less than 6 min seem to represent mechanical turbulence. Most of the turbulent energy created by thermal convection appears to be contained between frequencies with periods from 6 to 15 min. During stable atmospheric conditions, atmospheric undulations become important contributors to component velocity variance at frequencies with periods from 6 to greater than 60 min. The results of this study also indicate that a fundamental understanding of surface boundary layer turbulence processes cannot be achieved unless the three-dimensional character of these motions is studied.

2.6 Mesoscale Diffusion

Calculated total integrated concentration (TIC) values obtained from the mesoscale transport and puff diffusion model were compared to measured values sampled over the upper Snake River Plain. A part of this comparison was an examination of the puff diffusion estimates versus estimates from the Gaussian diffusion equation for a continuous point source. Figure 14 a and b illustrate the ratio of TIC versus travel distance for mean wind speeds of 1, 5, 10, and 25 m/sec. These curves are labeled for atmospheric diffusion categories (A through F) and for mean wind speed (e.g., 5D identifies the curve for 5 m/sec during category D conditions). The 25 m/sec wind speed curve approaches a reasonable estimate of an upper boundary (which technically doesn't exist) of the TIC ratios. These "errors" in the puff model calculations increase with greater wind speeds and with longer time lengths of effluent puff advection-steps. These "errors" also depend on the rate of horizontal effluent spreading and stratify according to diffusion category. Over the NRTS, the rate of horizontal spreading is largest for category A and least for category D (Yanskey et al., 1966). Thus, the ratio for category A values most rapidly approaches unity, while the ratio for category D least rapidly approaches unity. Figure 15 a and b illustrates the influence of the time-length of the puff advection steps. These curves illustrate the puff model "error of under-estimation" for category D diffusion rate and a mean wind speed of 25 mps. The individual curves are labeled for advection step lengths of 1, 2, 4, and 10 min. They indicate that the shorter the time-length of the advection step, the greater the reduction in the error at a given distance.

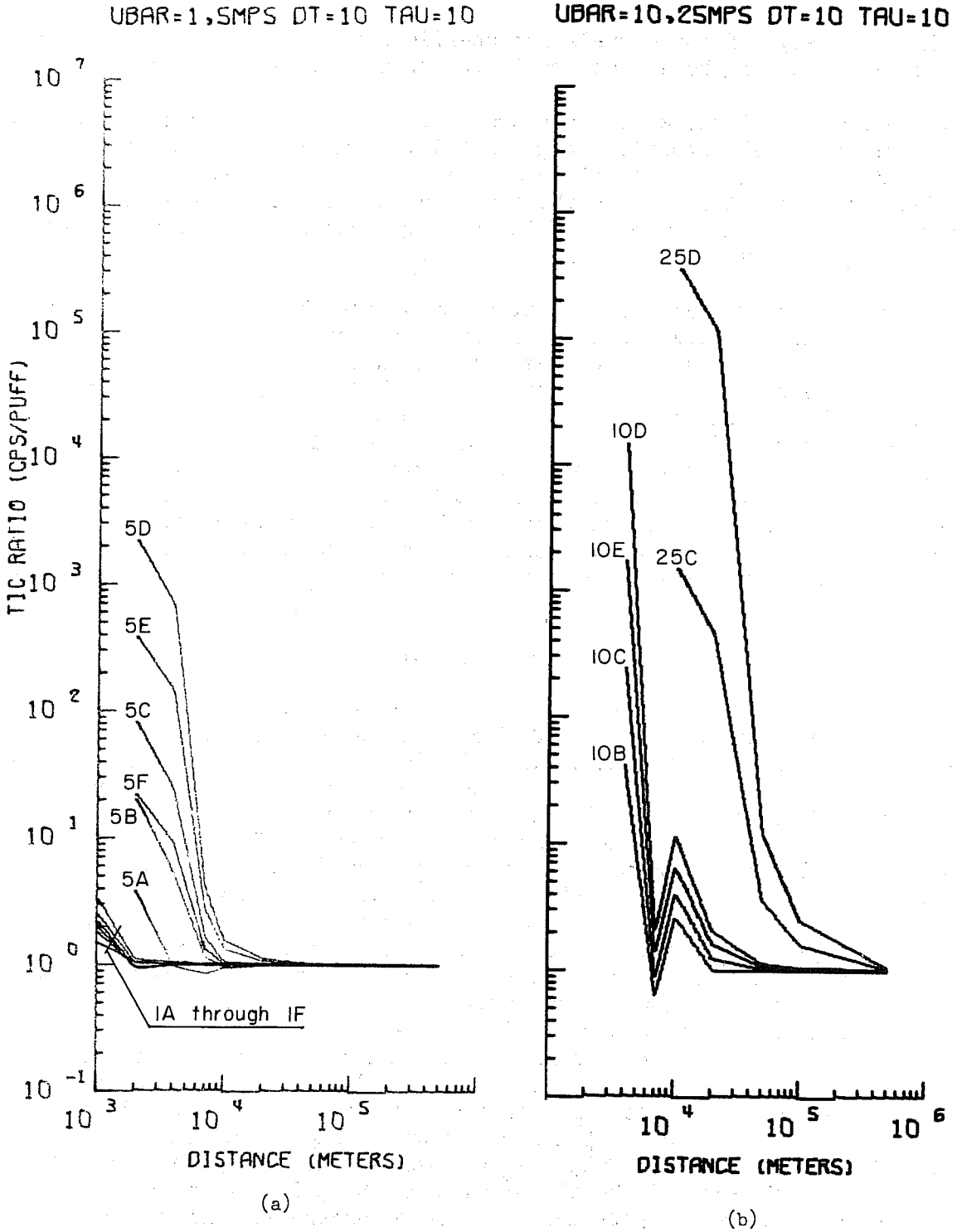

Figure 14. Ratio of Total Integrated Concentration (TIC) for 1 and 5 m/sec (a) and for 10 and 25 m/sec (b) computed from the continuous point source equation to TIC accumulated from the puff or instantaneous point source equation. The curves are labeled for the wind speed, in meters per second, and lettered for the NRTS stability class. The time length of advection steps is constant and equals 10 minutes.

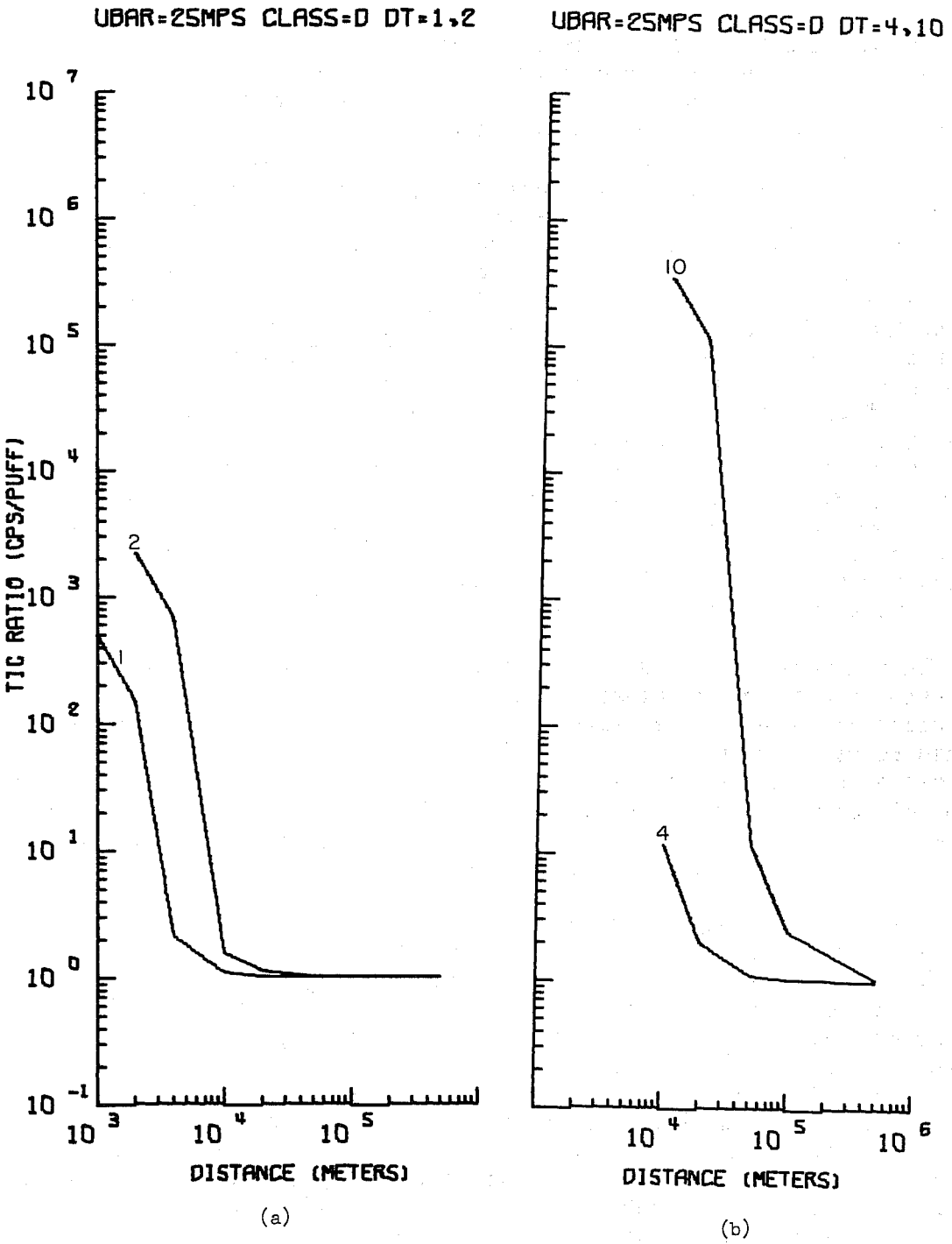

Figure 15. Ratio of Total Integrated Concentration (TIC) for 1 and 2 min (a) and for 4 and 10 min (b) advection steps, like in figure 14, except all curves apply to D stability class and 25 mps wind speed. Individual curves are labeled in minutes for different time lengths of advection steps.

To evaluate the model, measured 1-week integrated effluent concentrations were obtained for several points over the upper Snake River Plain. The effluent source was assumed to be the 250-ft stack at the Chemical Processing Plant located 3 mi to the north of the Central Facilities Area (CFA) shown in figure 4. In figures 16 and 17 the geographical distribution of the transport during the two 1-week periods is shown. Hypothetical particles were released, during each week, at the rate of one per hour and transported in the hourly averaged wind fields. Each individual trajectory was traced for 23 hr or until it left the computational area, whichever was the shorter. The trajectories are numbered sequentially for each consecutive 12-hr period during the week and letter symbols are located at 1-hr intervals along each trajectory. As a first approximation, the TIC values expected within the computational areas are proportional to the density of trajectory plots. The results of two comparisons are shown in table 4. The observed 1-week capture of effluent mass on air sampler filters is listed for nine locations surrounding the source. The locations are shown in figure 4 except for Butte City which is 3 mi east of Arco and TRA which is 5 mi northwest of CFA. The minimum or straight line distance between the source and the various receptors is listed in kilometers. The ratio of calculated to observed effluent mass collection is also shown. The units of these total integrated concentrations are Curie-Hour per cubic meter.

In all cases, the model calculated TIC values are less than the corresponding observed values. Within a circumference of 26 km of the source, the observed values ranged within a factor of about 10, whereas the calculated values ranged within a factor of 200. A relationship between the TIC ratios and distance from the source is shown by figure 18. Since the length of the dose delivering trajectories will generally exceed the straight line distance between the source and receptor, these slopes represent an upper limit on the TIC ratio versus distance relationship.

The effluent sampling data, which was used for comparison with the model calculations, were collected between May 24 and June 7, 1968. The weather during the first 2 and last 5 days of this period was rainy. Since the mesoscale transport and diffusion model does not include any allowance for atmospheric removal processes, effluent washout by precipitation would be expected to have reduced calculated concentrations. The same would be true of dry deposition effects. The model "errors of underestimation" were largely eliminated during these calculations by generating effluent puffs each 6 min and accumulating the influence of each puff at 2-min intervals. The average source strength, as provided by the plant operating personnel may not be sensitive enough for the model, especially if "bursts" of effluent releases occurred over short periods of time. This could have a rather complex effect on observed versus calculated ratio. It is possible that the model is more accurate at certain times in a diurnal cycle, especially in view of the fact that the model does not account for the directional shear often found in the vertical during nighttime inversion conditions. This further raises the question of the adequacy of the wind observation network to describe the wind patterns vertically as well as horizontally. The smaller range for the observed values raises the possibility that the cutting off of trajectories at the grid boundary or after 24 hours causes an underestimation of calculated values at greater distances. The remaining factor which may

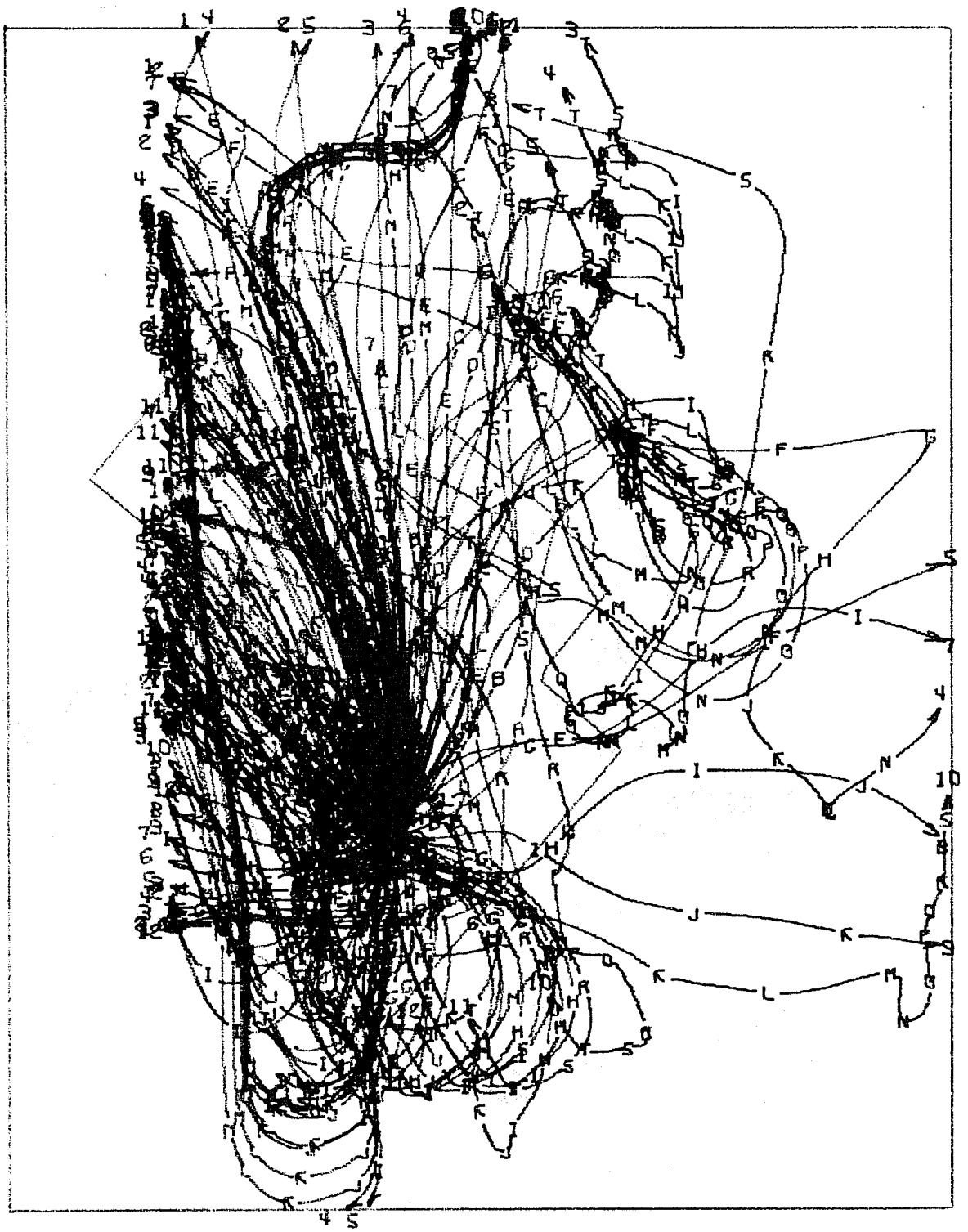

Figure 16. Geographical distribution of trajectories for the 168 hypothetical particles released during week #1, 1300 MST, May 24 to 1300 MST, May 31, 1968.

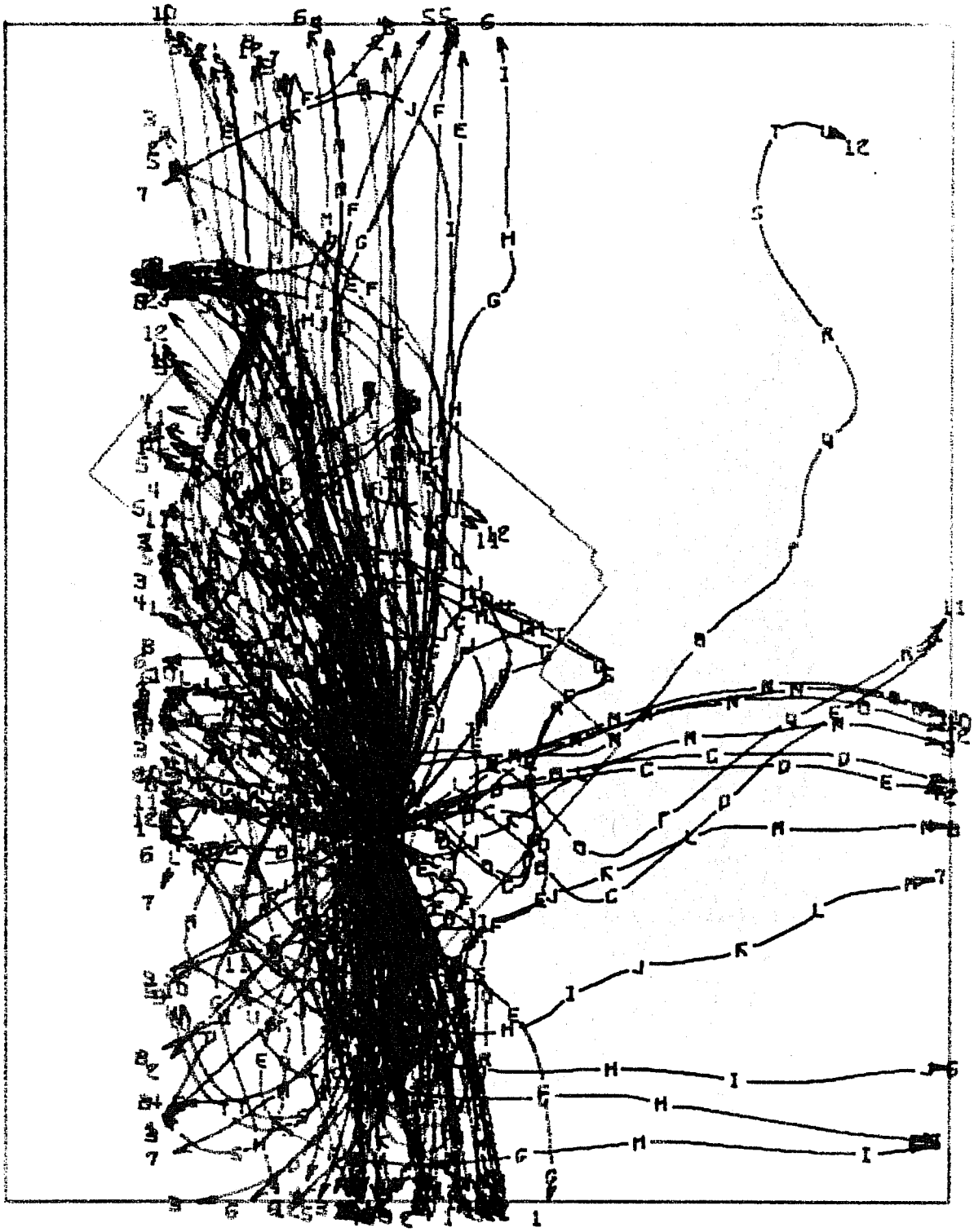

Figure 17. Geographical distribution of trajectories for the 168 hypothetical particles released during week # 2, 1300 MST, May 31 to 1300 MST, June 7, 1968.

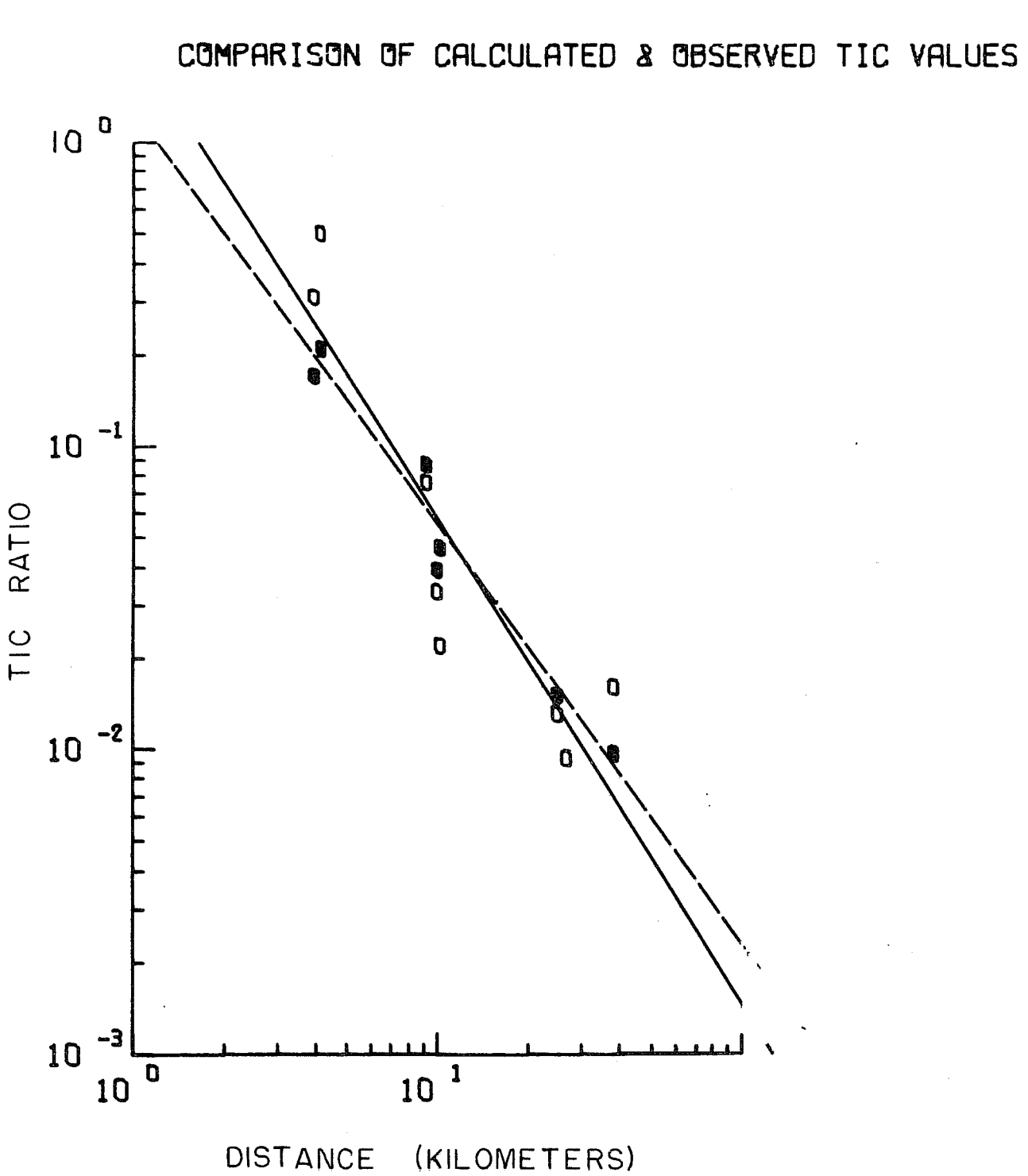

Figure 18. Ratio of model calculated TIC to field sampled TIC values versus straight line distance to receptors (in kilometers). The dots represent data points for week # 1 and are fitted with a dashed regression line with slope -1.4. The circles represent data points for week # 2 and are fitted with the solid regression line of slope -1.6.

Table 4. Comparison of Calculated and Observed TIC Values

	Week #1								
	Butte City	EBR I	CFA	TRA	NRF	TAN	SPERT	EBR II	Idaho Falls
TIC Calculated	-	6.7×10^{-12}	2.4×10^{-11}	3.3×10^{-11}	1.1×10^{-11}	9.9×10^{-13}	4.8×10^{-12}	6.4×10^{-13}	0.0
TIC Observed	-	1.5×10^{-10}	1.1×10^{-10}	1.9×10^{-10}	2.8×10^{-10}	1.0×10^{-10}	5.5×10^{-11}	4.4×10^{-11}	0.0
TIC Ratio		4.6×10^{-2}	2.1×10^{-1}	1.7×10^{-1}	3.9×10^{-2}	9.7×10^{-3}	8.7×10^{-2}	1.5×10^{-2}	-
	Week #2								
TIC Calculated	2.8×10^{-13}	7.8×10^{-12}	1.6×10^{-11}	6.3×10^{-11}	1.0×10^{-11}	5.2×10^{-13}	2.8×10^{-12}	4.2×10^{-13}	3.0×10^{-16}
TIC Observed	3.0×10^{-11}	3.5×10^{-10}	3.2×10^{-10}	2.0×10^{-10}	3.0×10^{-10}	3.7×10^{-11}	3.7×10^{-11}	3.2×10^{-11}	$\leq1.2\times10^{-11}$
TIC Ratio	9.3×10^{-3}	2.2×10^{-2}	5.0×10^{-1}	3.1×10^{-1}	3.3×10^{-2}	1.6×10^{-2}	7.6×10^{-2}	1.3×10^{-2}	-
Minimum Distance (km)	26.4	10.1	4.1	3.9	9.9	37.7	9.1	24.5	75.5

affect the observed versus calculated ratios is an error in estimating vertical and horizontal spreading. In the model, vertical diffusion as defined by the parameter, σ_z, is limited by the depth of the vertical mixed layer, and thus cannot contribute to the underestimation of calculated values. The original assumptions in the model concerning the horizontal diffusion parameter, σ_y, were the following:

(A) The short range diffusion measurements (downwind to a few kilometers) provide an empirical estimate of the distance dependence of σ_y and this dependence can be extrapolated into the mesoscale.

(B) The mesoscale has its own dispersive effect (trajectory meandering), which can be incorporated through use of a wind field that varies in space and time.

There is the distinct possibility that empirical estimates of the growth rate of σ_y with distance is not appropriate for extension into the mesoscale - at least not at full value. It may be that within distances of a few kilometers, the σ_y growth rate is closely tied with turbulence and buoyancy forces extending up to an hour and that the extension of this growth rate into the region corresponding to the mesoscale gap of the turbulent energy spectrum (Van der Hoven, 1957) is not valid.

The number of possible sources of error in the mesoscale transport and diffusion model and in the parameters of the model makes it difficult to identify with confidence the reason for the discrepancy between calculated and observed concentrations for the 2-week test period. Additional cases need to be examined. Furthermore, controlled tracer releases and concentration measurements within the mesoscale computational area are needed to support a verification check of the model. The verification program should be based on observations of concentration which have a time resolution of the same order as the parameters in the model, that is, hourly values.

3. REFERENCES

ESSA Tech. Memo. ERLTM-ARL 5 (1968), Atmospheric transport and diffusion in the planetary boundary layer, Air Resources Laboratories Semiannual Research Program Review for the Division of Reactor Development and Technology, USAEC, 60 pp.

ESSA Tech. Memo. ERLTM-ARL 9 (1968), Atmospheric transport and diffusion in the planetary boundary layer, Air Resources Laboratories Semiannual Research Program Review for the Division of Reactor Development and Technology, USAEC, 60 pp.

ESSA Tech. Memo. ERLTM-ARL 14 (1969), Atmospheric transport and diffusion in the planetary boundary layer, Air Resources Laboratories Semiannual Research Program Review for the Division of Reactor Development and Technology, USAEC, 44 pp.

Markee, E. H., contributor, (1968), Controlled Environmental Radioiodine Tests, U. S. Atomic Energy Commission, Progress Report No. 3, IDO-12063, 77 pp.

Markee, E. H., contributor, (1969), Controlled Environmental Radioiodine Tests, U. S. Atomic Energy Commission, Progress Report No. 4, IDO-12065, 78 pp.

Slade, D. H., editor, (1968), Meteorology and Atomic Energy, U. S. Atomic Energy Commission Technical Information Document, TID-24190, 445 pp.

Van der Hoven, I., (1957), Power Spectrum of Horizontal Wind Speed in the Frequency Range from 0.0007 to 900 Cycles per Hour, J. of Meteorol. 14, No. 2, 160-164.

Yanskey, G. R., E. H. Markee, A. P. Richter, (1966), Climatography of the National Reactor Testing Station, U. S. Atomic Energy Commission, IDO-12048, 184 pp.

4. REVIEW OF REACTOR SAFETY ANALYSIS REPORTS

The Air Resources Laboratories in Silver Spring, Maryland, and the Field Office in Idaho have continued to take an active part in the review of reactor safety analysis reports as well as consultations with regard to the preparation of the reports. In addition, written comments have been prepared for the Division of Reactor Licensing through the Division of Reactor Development and Technology as follows:

1. Indian Point Nuclear Generating, Unit No. 3, Consolidated Edison Company of New York, Inc. Preliminary Safety Analysis Report, Supplement 5, dated November 4, 1968.

2. Monticello Nuclear Generating Plant, Unit 1, Northern States Power Company Final Safety Analysis Report, Volumes I, II, III, and IV, dated October 17, 1968.

3. Barnwell Nuclear Fuel Plant, Allied Chemical Nuclear Products, Inc. Safety Analysis Report, Volumes I and II, dated November 7, 1968.

4. Duane Arnold Energy Center, Iowa Electric Light and Power Company Preliminary Safety Analysis Report, Volumes I through VI, dated November 4, 1969 and Amendment No. 1 dated December 24, 1968.

5. Palisades Plant Consumers Power Company Final Safety Analysis Report, Volumes I, II, and III, dated November 1, 1968.

6. Midland Plant, Units 1 and 2, Consumers Power Company Preliminary Safety Analysis Report, Volumes I and II, dated October 30, 1968.

7. H. B. Robinson, Unit No. 2, Carolina Power and Light Company Final Facility Description and Safety Analysis Report, Volumes I, II, and III, dated November 26, 1968.

8. James A. Fitzpatrick Nuclear Power Plant, Power Authority of the State of New York Preliminary Safety Analysis Report, Volumes I, II, and III, dated December 31, 1968.

9. Beaver Valley Power Station, Duquesne Light Company Preliminary Safety Analysis Report, Volumes I, II, and III, dated January 13, 1969.

10. Three Mile Island Nuclear Station, Unit 2, Metropolitan Edison Company and Jersey Central Power and Light Company Preliminary Safety Analysis Report, Volumes I, II, III, and IV, dated March 10, 1969.

11. Hutchinson Island Plant, Unit No. 1, Florida Power and Light Company Preliminary Safety Analysis Report, Volumes I, II, and III, dated January 29, 1969.

12. FBR Demonstration Plant, General Public Utilities/Pennsylvania Electric Co. and North American Rockwell/atomics International Division Safety Analysis, Volumes I and II, dated May 6, 1968.

13. North Anna Power Station, Units 1 and 2, Virginia Electric and Power Company Preliminary Safety Analysis Report, Volumes I, II, III, and IV, dated March 21, 1969.

14. Point Beach Nuclear Plant, Unit 1 and 2, Wisconsin Electric Power Company and Wisconsin Michigan Power Company Final Facility Description and Safety Analysis Report, Volumes I, II, III, and IV, dated March 14, 1969.

15. Seabrook Nuclear Station, Unit No. 1, Public Service Company of New Hampshire, The United Illuminating Company Preliminary Safety Analysis Report, Volumes I, II, and III, dated April 9, 1969.

16. Duane Arnold Energy Center, Iowa Electric Light and Power Company Preliminary Safety Analysis Report, Amendment No. 3, dated May 2, 1969.

17. Shoreham Nuclear Power Station, Long Island Lighting Company Preliminary Safety Analysis Report, Amendments 4 and 5, dated April 28, 1969.

18. Palisades Plant, Consumers Power Company Final Safety Analysis Report, Amendment No. 12, dated May 14, 1969.

5. PUBLICATIONS

1. Dickson, C. R., G. E. Start, and E. H. Markee, "Aerodynamic Effects of the EBR-II Reactor Complex on Effluent Concentration," Nuclear Safety, 10, No. 3, 228-242, May-June 1969.

2. Slade, D. H., "Wind Measurement on a Tall Tower in Rough and Inhomogeneous Terrain," J. of Appl. Meteorol., 8, No. 2, 293-297, April 1969.

3. Van der Hoven, I., "Wind Persistence Probability," ESSA Tech. Memo. ERLTM-ARL 10, 32 pp, February 1969.

6. LABORATORY PERSONNEL

Silver Spring, Maryland

Abram B. Bernstein, meteorologist, returned to duty on January 30, 1969 after completion of the fall-winter term of graduate study at the University of Washington, Seattle, Washington.

David H. Slade, meteorologist, was temporarily assigned on February 3, 1969, to the Fallout Studies Branch, U. S. Atomic Energy Commission, Germantown, Maryland.

Idaho Falls, Idaho

Hal Shearer and Steve Manning entered on duty May 7, 1969, as student assistants under the Junior Fellowship Program.

Regina Young accepted summer employment on May 26, 1969 through the Youth Opportunity Program.

Dr. Gale Biggs, Iowa State University, visited and worked at the Research Office from March 27 through April 4, 1969.